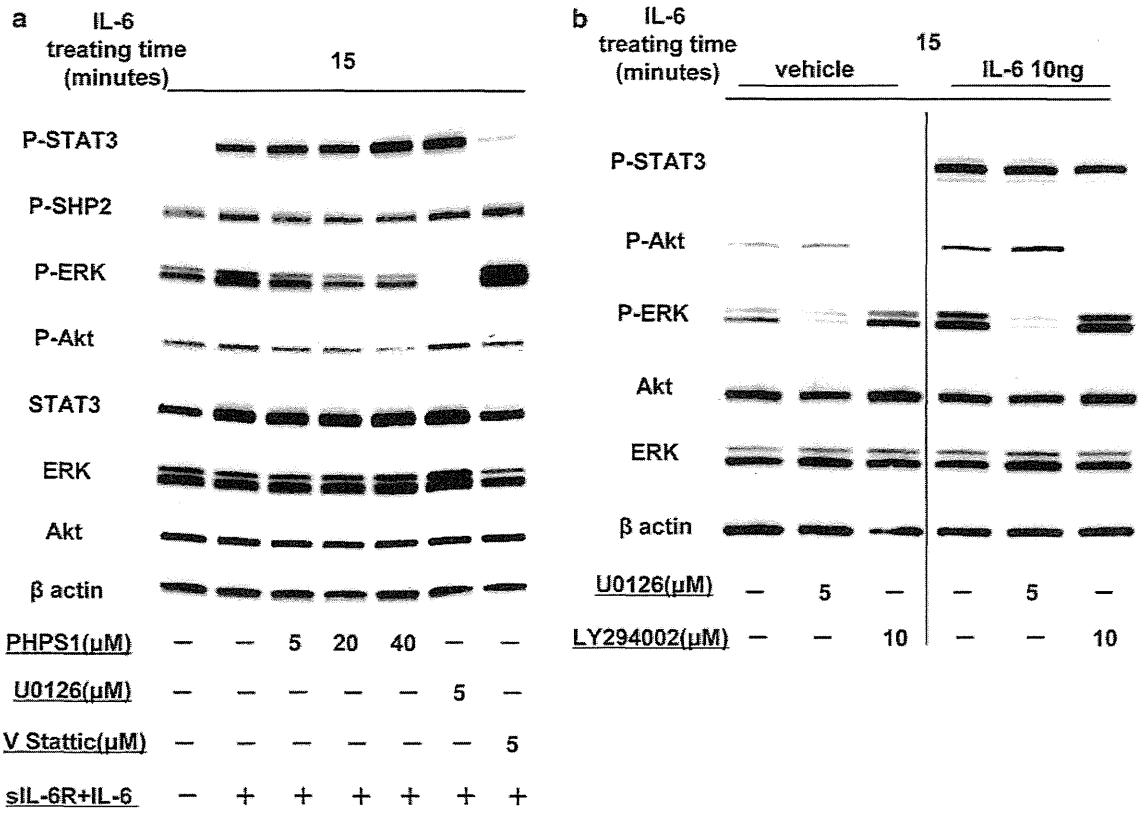

Fig. 4 IL-6-induced activation of ERK was enhanced by blocking the STAT3 signaling pathway, and IL-6-induced ERK and Akt signaling pathways negatively regulated each other reciprocally. **a** MC3T3-E1 cells were stimulated with 10 ng/ml IL-6 and 100 ng/ml sIL-6R (15 min) after pretreatment either with PHPS1 (5, 20, 40 μM; 1 h), with U0126 (5 μM; 1 h), or with V Stattic (5 μM; 1 h), and the cell lysates were subjected to Western blotting. PHPS1 inhibited IL-6-induced phosphorylation of ERK and Akt to the constitutive level, but not of STAT3. IL-6-induced activation of ERK was enhanced by V Stattic. **b** MC3T3-E1 cells were treated with vehicle or with 10 ng/ml IL-6 and 100 ng/ml sIL-6R (15 min) after pretreatment either with U0126 (5 μM; 1 h) or with LY294002 (10 μM; 1 h), and the cell lysates were subjected to Western blotting. Both constitutive and IL-6-induced phosphorylation of Akt and ERK were enhanced by treatment with U0126 and LY294002, respectively. Representative data from at least three independent experiments are shown

The negative effect of IL-6/sIL-6R on the expression of osteoblastic genes (Runx2, osterix and osteocalcin) was also restored by treatment with either U0126, LY294002, or PHPS1 in a dose-dependent manner, while it was enhanced by treatment with V Stattic (Fig. 5b). Moreover, a high dose of PHPS1, 20 μM, caused significantly upregulated expression of osteocalcin.

For mineralization of ECM, the negative effect of IL-6/sIL-6R was restored by treatment with either U0126, LY294002, or PHPS1. As with ALP activity and osteoblastic gene expression, the negative effect of IL-6/sIL-6R on mineralization was enhanced by treatment with V Stattic (Fig. 6a, b). ALP activity, osteoblastic gene expression, and mineralization of ECM in cells treated only with each inhibitor demonstrated the same behavior (Figs. 5, 6).

Furthermore, the negative effects of ALP activity, osteoblastic gene expression and mineralization of ECM by stimulation with IL-6/sIL-6R were compared for levels in the presence and in the absence of each inhibitor. The negative effects on osteoblast differentiation by IL-6/sIL-6R showed a tendency to decrease in the presence of each inhibitor, as compared to the absence of inhibitors (Figs. 5, 6). The negative effects were decreased by 15–44, 20–61, 7–140, and 21–80 % in the presence of U0126, LY294002, PHPS1 and V Stattic, respectively, as compared to the absence of inhibitors. These results indicate that the effects of IL-6/sIL-6R on osteoblast differentiation might be mediated either by MEK/ERK, PI3K/Akt, or JAK/STAT3 pathways.

Knockdown of MEK2 and Akt2 via siRNA transfection restores ALP activity and Runx2 gene expression

To further confirm the effects of MEK and Akt inhibition on osteoblast differentiation in MC3T3-E1 cells, we studied cell differentiation after knockdown of MEK and Akt. For each protein, RNAs of two isoforms were separately blocked: MEK1 and MEK2 for MEK, and Akt1 and Akt2 for Akt.

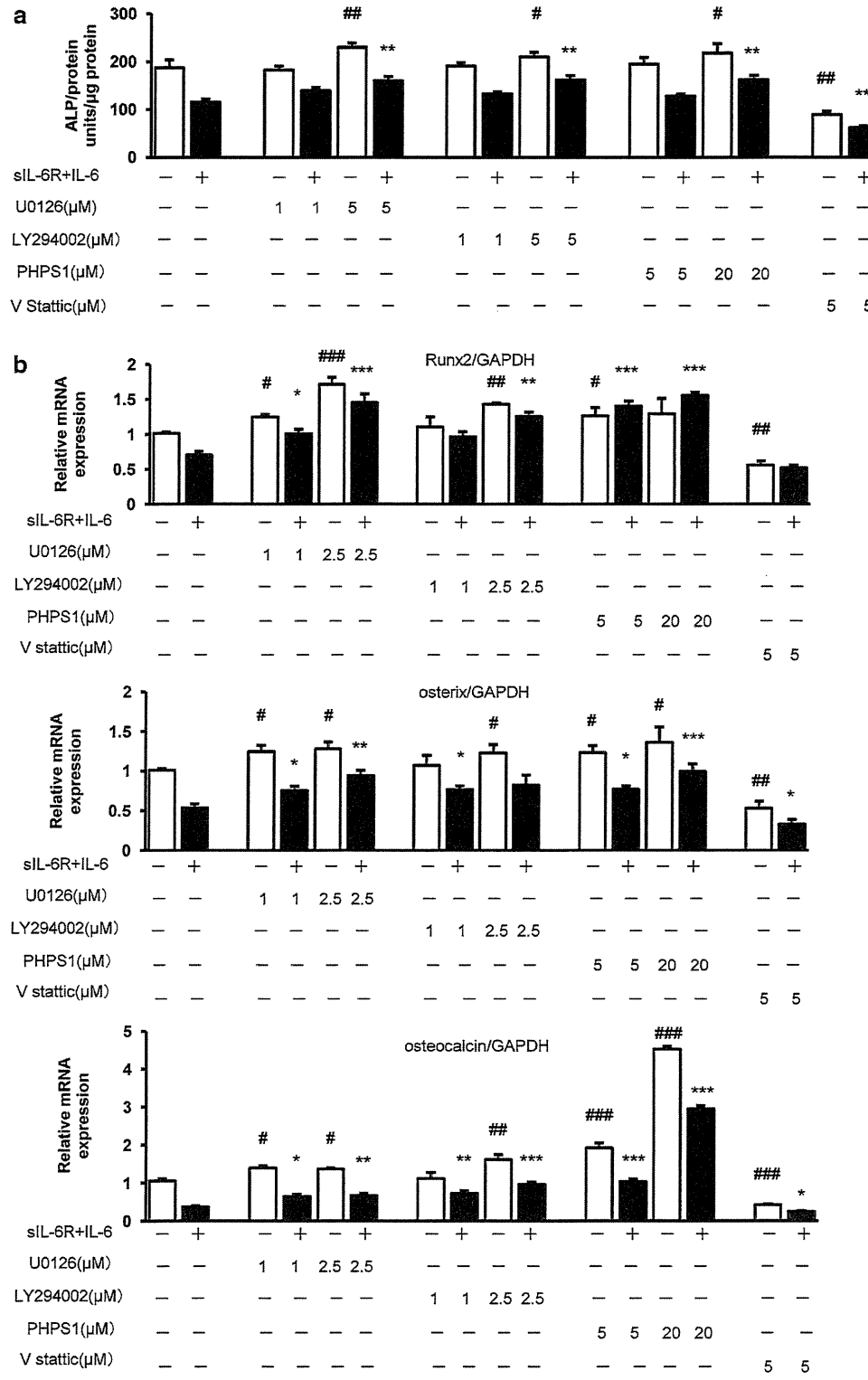

Fig. 5 The negative effects of IL-6 on ALP activity and the expression of osteoblastic genes were restored by inhibition of MEK, PI3K, and SHP2, while they were enhanced by inhibition of STAT3. MC3T3-E1 cells were pretreated either with U0126 (1, 2.5, 5 μM; 1 h), LY294002 (1, 2.5, 5 μM; 1 h), PHPS1 (5, 20 μM; 1 h), or V Stattic (5 μM; 1 h), then stimulated either with 10 ng/ml IL-6 and 100 ng/ml sIL-6R or with vehicle and incubated for 6 days. (a) ALP activity of the cell lysates was measured using p-nitrophenylphosphate as a substrate. The negative effect of IL-6 on ALP activity was restored by treatment with either U0126, LY294002, or PHPS1 in a dose-dependent manner, while it was enhanced with V Stattic. **b** Total RNA was extracted and real-time PCR for Runx2, osterix, and osteocalcin was performed. Data were normalized to GAPDH expression and are shown as the ratio of gene expression compared to control cells treated with vehicle. The negative effect of IL-6 on expression of osteoblastic genes was restored by treatment either with U0126, LY294002, or PHPS1 in a dose-dependent manner, while it was enhanced by treatment with V Stattic. Representative data from at least three independent experiments are shown. Data are shown as mean ± SE. *n.s.* not significant; $^{\#}P < 0.05$; $^{\#\#}P < 0.001$; $^{\#\#\#}P < 0.001$, compared to the group treated with vehicle. $^{*}P < 0.05$; $^{**}P < 0.001$; $^{***}P < 0.001$, compared to group treated with IL-6/sIL-6R

The protein expression level of each molecule was found to be diminished selectively at 48 h after transfection of the respective siRNAs (Fig. 7a). The ALP activity in MC3T3-E1 cells treated with IL-6/sIL-6R was restored by knockdown of MEK2 and Akt2 as compared to that in cells transfected with negative control siRNA. On the other hand, knockdown of MEK1 and Akt1 enhanced the negative effects of IL-6/sIL-6R on ALP activity (Fig. 7b) (ALP activity after transfection with each siRNA without IL-6/sIL-6R demonstrated the same behavior; Fig. 7b) Quantitative real-time PCR analysis revealed that the gene expressions of Runx2, osterix, and

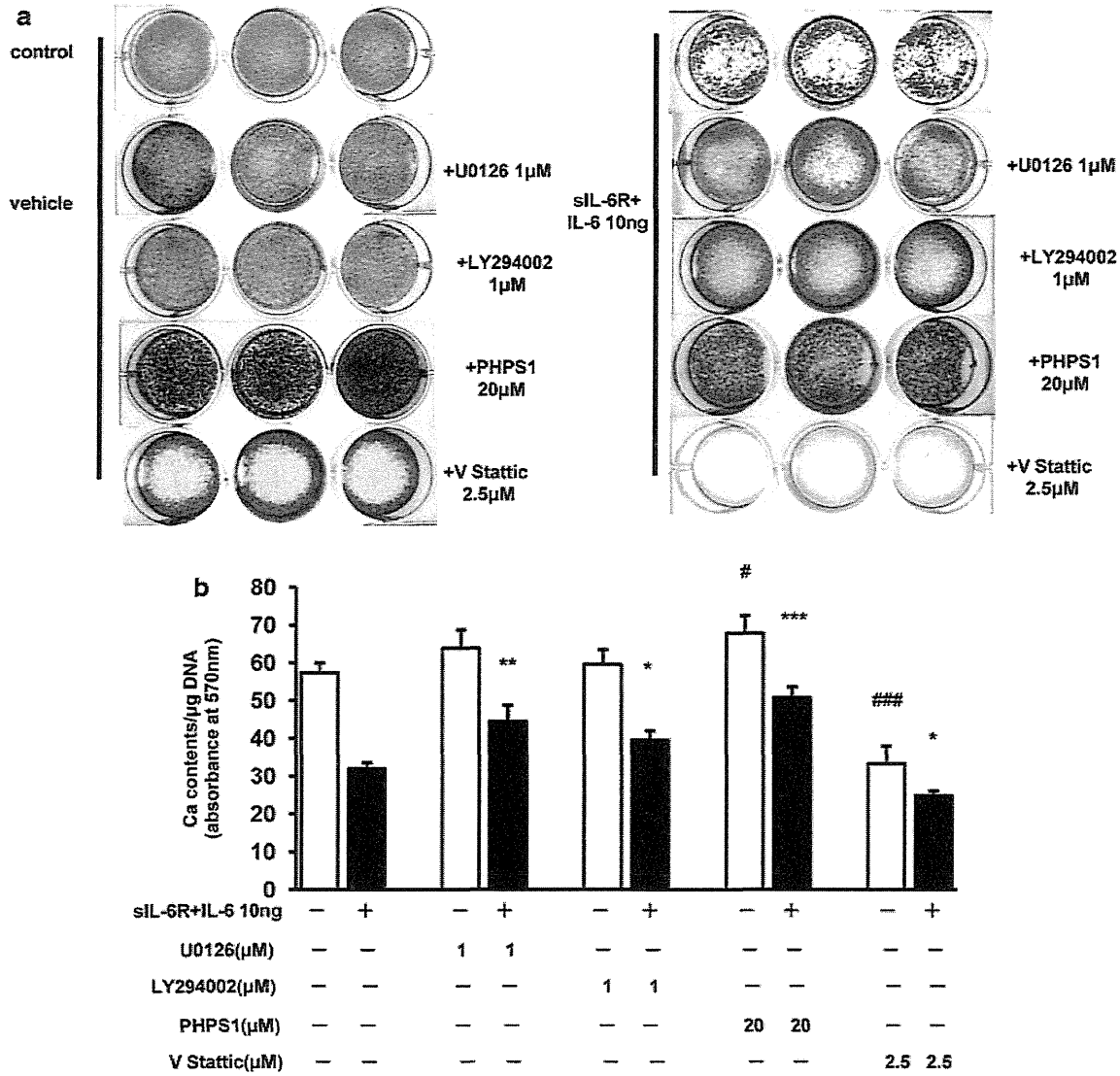

Fig. 6 The negative effect of IL-6 on mineralization of ECM was restored by inhibition of MEK, PI3K, and SHP2, while it was enhanced by inhibition of STAT3. MC3T3-E1 cell were pretreated either with U0126 (1 μM; 1 h), LY294002 (1 μM; 1 h), PHPS1 (20 μM; 1 h), or V Stattic (2.5 μM; 1 h), then stimulated with either 10 ng/ml IL-6 and 100 ng/ml sIL-6R or with vehicle and incubated for 21 days. **a** After fixation, the cells were stained with alizarin red solution. The reduction of alizarin red staining by IL-6/sIL-6R was restored in cells treated with either U0126, LY294002, or PHPS1, while it was enhanced in those treated with V Stattic. **b** Quantification of matrix mineralization was by measurement of absorbance for alizarin red normalized by total DNA content. The reduction of matrix mineralization by IL-6/sIL-6R was restored in cells treated with either U0126, LY294002, or PHPS1, while it was enhanced in those treated with V Stattic. Representative data from at least three independent experiments are shown. Data are shown as mean ± SE. *n.s.* not significant; $^{\#}P < 0.05$; $^{\#\#}P < 0.001$; $^{\#\#\#}P < 0.001$, compared to the group treated with vehicle. $^{*}P < 0.05$; $^{**}P < 0.001$; $^{***}P < 0.001$, compared to group treated with IL-6/sIL-6R

osteocalcin were restored by knockdown of MEK2. On the other hand, knockdown of Akt2 also restored Runx2, but decreased osteocalcin expression (Fig. 7c), while knockdown of Akt2 without IL-6/sIL-6R caused no significant difference in Runx2 expression (Fig. 7b). As was recognized for ALP activity, knockdown of MEK1 and Akt1 enhanced the downregulation of osteocalcin expression (Fig. 7b, c). Also, the negative effects of IL-6/sIL-6R on osteoblast differentiation showed some tendency to decrease with each knockdown compared to those without knockdown. The negative effects were decreased by 2–24, 4–27, 7–43, and 21–26 % with knockdown of MEK1, MEK2, Akt1, and Akt2, respectively, as compared to those without knockdown. These results indicate that IL-6 may suppress osteoblast differentiation through MEK2 and Akt2.

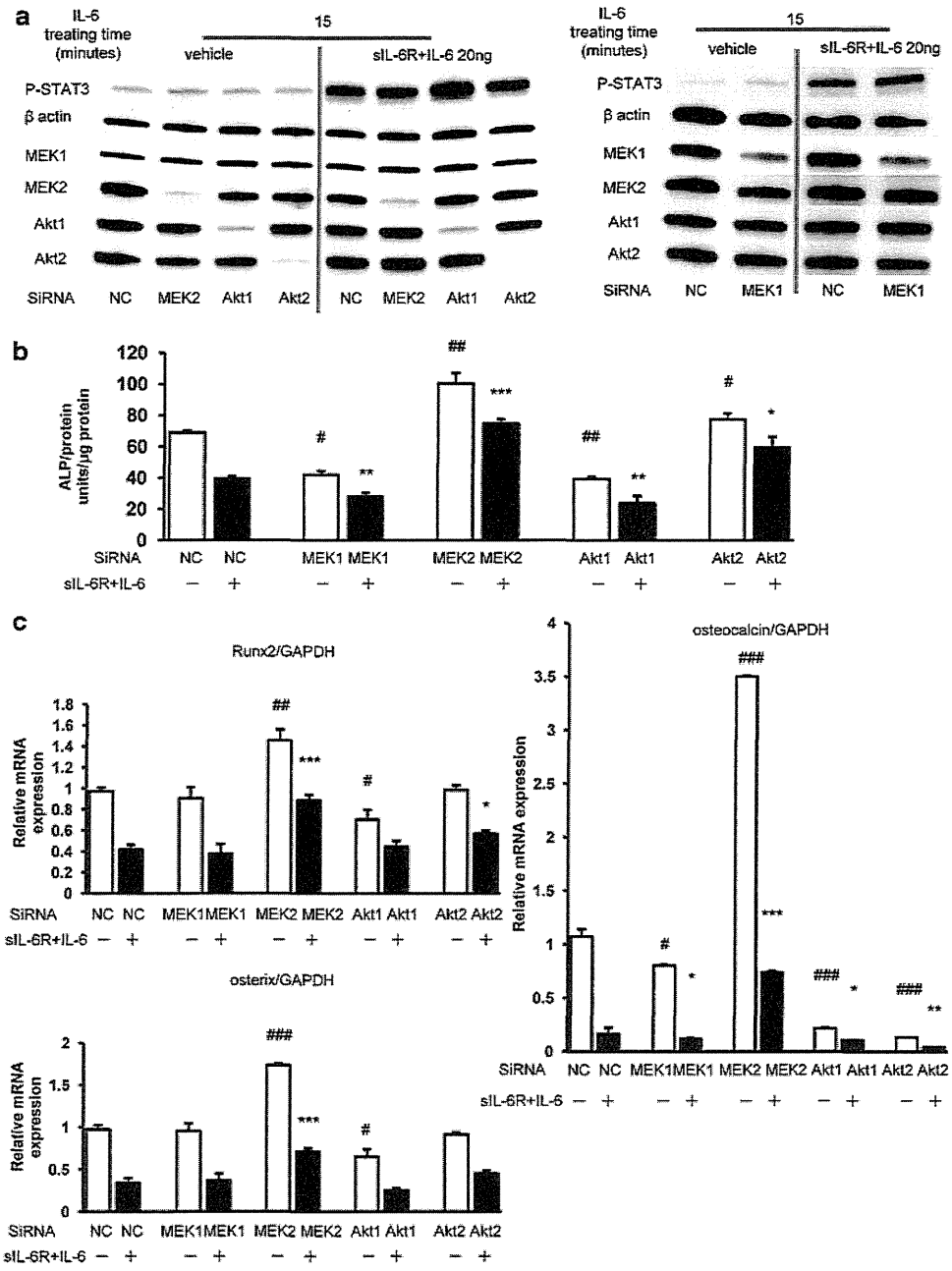

Fig. 7 Knockdown of MEK2 and Akt2 in cells transfected with siRNA restored ALP activity and Runx2 gene expression. **a** MC3T3-E1 cells transfected with respective siRNAs were cultured for 48 h. Western blotting was performed using cell lysates stimulated with vehicle or with 20 ng/ml IL-6 and 100 ng/ml sIL-6R (15 min). Expression levels of each protein, MEK1, MEK2, Akt1, and Akt2, were selectively diminished at 48 h after transfection with respective siRNAs. **b** MC3T3-E1 cells transfected with respective siRNAs were incubated for 48 h after which the medium was changed to differentiation medium with vehicle or with 20 ng/ml IL-6 and 100 ng/ml sIL-6R. The cells were then incubated for 3 days to evaluate osteoblast differentiation. ALP activity in MC3T3-E1 cells treated with IL-6/sIL-6R was restored by knockdown of MEK2 and Akt2 as compared to that in cells transfected with negative control siRNA. **c** Expression of osteoblastic genes in MC3T3-E1 cells transfected with respective siRNAs was assessed by real-time PCR. The expression of each gene was normalized against GAPDH expression. The gene expressions of Runx2, osterix, and osteocalcin were restored by knockdown of MEK2. Knockdown of Akt2 also restored Runx2, but decreased osteocalcin. Representative data from at least three independent experiments are shown. Data are shown as mean ± SE. *n.s.* not significant; $^{\#}P < 0.05$; $^{\#\#}P < 0.001$; $^{\#\#\#}P < 0.001$, compared to negative control group treated with vehicle. $^{*}P < 0.05$; $^{**}P < 0.001$; $^{***}P < 0.001$, compared to negative control group treated with IL-6/sIL-6R

IL-6/sIL-6R inhibits the differentiation of primary murine calvarial osteoblasts by activating phosphorylation of ERK, Akt2, and STAT3

Experiments were repeated with murine calvarial osteoblasts isolated from the calvariae of 3-day-old C57BL/6 mice. As was recognized in MC3T3-E1 cells, IL-6 inhibited ALP activity (Fig. 8a), the expression of osteoblastic genes (Fig. 8b), and mineralization (Fig. 8c, d) in a dose-dependent manner. Furthermore, IL-6 induced phosphorylation of ERK, Akt2, and STAT3 (Fig. 8e), which was exactly the same as with MC3T3-E1 cells.

Discussion

We examined the effects of IL-6 and its soluble receptor on the proliferation and differentiation of murine MC3T3-E1 osteoblastic cells and primary murine calvarial osteoblasts. Our results showed that they significantly reduced ALP activity, bone mineralization, and expression of the osteoblastic genes Runx2 osterix and osteocalcin, in a dose-dependent manner. From these experiments, we clearly demonstrated that IL-6 inhibited osteoblast differentiation of MC3T3-E1 cells and primary murine calvarial osteoblasts.

It has been demonstrated that the JAK/STAT3 signaling pathway has important roles both, in vivo and in vitro, in the differentiation of osteoblasts [37, 38]. Our results are consistent with previous reports and imply that the activation of STAT3 induced by IL-6 may induce osteoblast differentiation.

IL-6 activates another major intracellular signaling pathway, SHP2/ERK, and can also lead to the activation of an additional signaling cascade involving SHP2/PI3K/Akt. IL-6-induced activation of PI3K and downstream protein kinase Akt/PKB has been reported to play important roles in the proliferation of prostate cancer cells [30, 31], hepatoma cells [32], and multiple myeloma cells [29]. They were also reported to associate with neuroendocrine differentiation of prostate cancer cells induced by IL-6 [32]. In this study, we focused on the PI3K/Akt pathway triggered by IL-6, because no reports have demonstrated the role of IL-6 in the activation of PI3K/Akt signaling pathway in osteoblasts. We have demonstrated for the first time that IL-6-induced activation of Akt2, one of the downstream pathways of SHP2, may be a key player in the negative regulation of osteoblast differentiation induced by IL-6. Among the three isoforms of Akt, Akt1 and Akt2 are highly expressed in osteoblasts [39]. Mice lacking Akt1, the major isoform in bone tissue, exhibit osteopenia [40, 41], and the impact of Akt1 deficiency in osteoblast differentiation and bone development have also been published [39, 42–44], all of which are consistent with our results showing that knockdown of Akt1 signaling by siRNA inhibited osteoblast differentiation. In contrast, Mukherjee et al. [44] reported enhanced osteogenic differentiation in the absence of Akt1 in cell lines. Moreover, they reported that Akt2 was required for BMP2-initiated osteoblast differentiation of cultured murine mesenchymal stem cells, but that Akt1 was dispensable in this assay [45], which is inconsistent with our results showing that knockdown of Akt2 signaling by siRNA promoted osteoblast differentiation. These discrepancies might be due to the difference between cell types, i.e. intramembranous (calvariae) cells and endochondral (long bones) cells.

In this study, gene expression of osteocalcin, a late osteoblastic differentiation marker, was upregulated by treatment with a PI3K/Akt inhibitor, but was downregulated by knockdown of both Akt1 and Akt2. Moreover, a complete blockade with a high dose (more than 10 μM) of the PI3K/Akt inhibitor conversely downregulated the expression of osteocalcin (data not shown). This discrepancy may be due to the difference between the temporary or partial blockade by the inhibitor and constitutive knockdown by siRNA. Since bone formation has been reported to increase without impairment of mineralization and resorption even in osteocalcin-deficient mice [46], the expression of osteocalcin may not directly affect bone formation.

We have previously reported that osteoblast differentiation was significantly promoted by MEK inhibitor in BMP-2-treated C2C12 cells and MC3T3-E1 cells [47]. Our findings in the present study are consistent with our previous report and others [47–49] at the point that IL-6-induced activation of ERK significantly downregulated osteoblast differentiation. In addition, our results suggest that there might be different roles in osteoblast differentiation between MEK1 and MEK2. Constitutively active expression of MEK1 has been reported to accelerate bone development both in vitro [50] and in vivo [51], which is consistent with the results showing that knockdown of MEK1 inhibited osteoblast differentiation in the present study. As for MEK2, there are no reports concerning its roles in osteoblast differentiation, and we are the first to demonstrate that MEK2 may also be a key player in the negative regulation of osteoblast differentiation induced by IL-6. The effects of an MEK inhibitor that inhibits both MEK1 and MEK2 on bone formation are still controversial [52]. These controversies might be due to different roles played between MEK1 and MEK2 in osteoblast differentiation, and the effects of MEK inhibitors could depend on which pathway is predominantly inhibited in each study.

With respect to intracellular signaling pathways, our results showed that IL-6 triggers three signaling pathways, one of which has a conflicting function with the others.

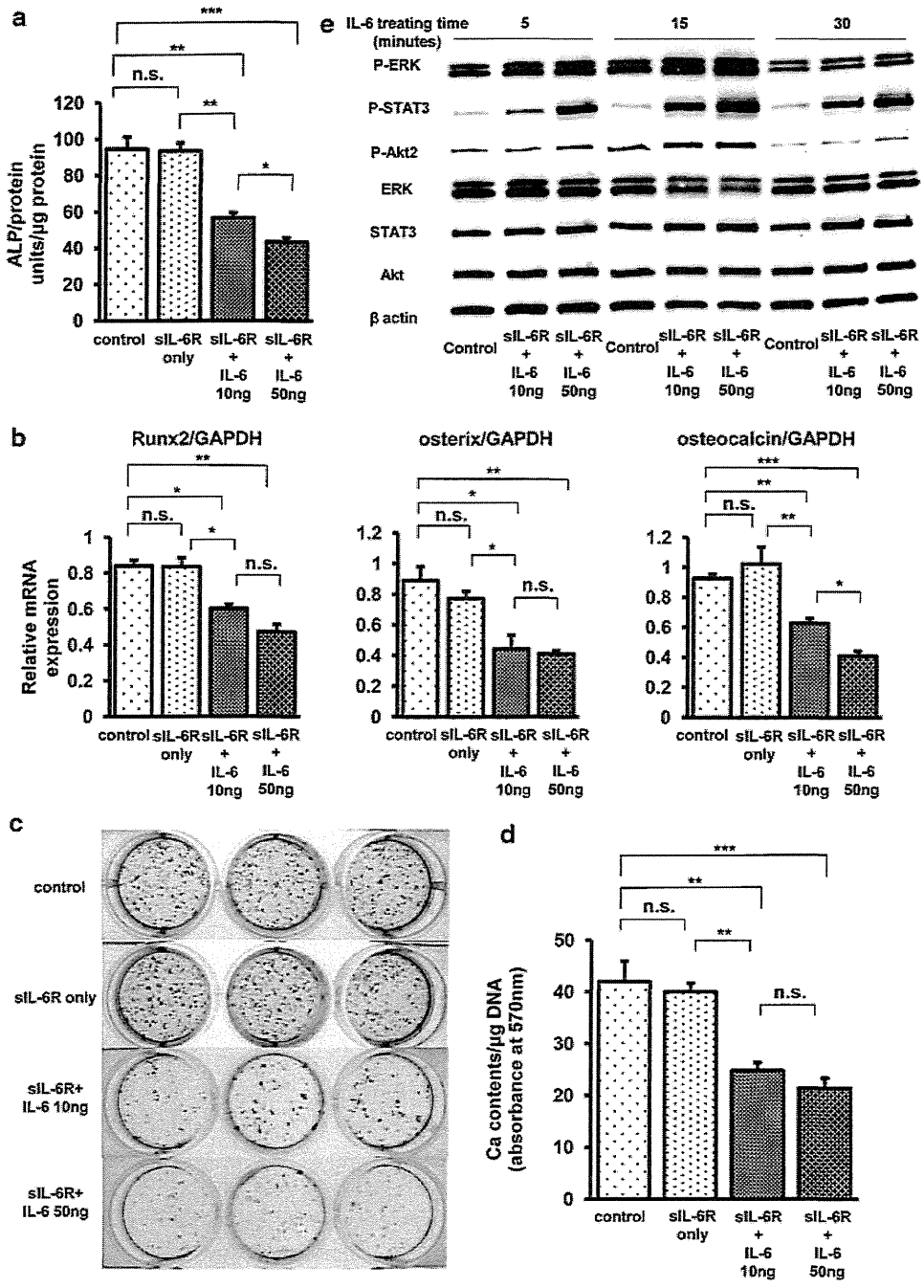

Fig. 8 IL-6/sIL-6R inhibited the differentiation of primary murine calvarial osteoblasts with the activated phosphorylation of ERK, Akt2, and STAT3. **a** ALP activity of lysates of murine calvarial osteoblasts treated with or without IL-6/sIL-6R for 6 days was measured using p-nitrophenylphosphate as a substrate. IL-6/sIL-6R significantly reduced ALP activity in a dose-dependent manner. **b** Total RNA was extracted from murine calvarial osteoblasts treated with or without IL-6/sIL-6R for 6 days, and real-time PCR for Runx2, osterix, and osteocalcin was performed. Data were normalized to GAPDH expression and are shown as the ratio of gene expression as compared to control cells treated with vehicle. The expression of osteoblastic genes was significantly downregulated by IL-6/sIL-6R in a dose-dependent manner. **c** Murine calvarial osteoblasts were treated with or without IL-6/sIL-6R and were cultured for 21 days. After fixation, the cells were stained with alizarin red solution. Apparently significant reduction of alizarin red staining was recognized in cells treated with either 10 or 50 ng/ml IL-6. **d** Matrix mineralization was quantified by measurement of absorbance for alizarin red normalized by total DNA content. IL-6/sIL-6R significantly inhibited mineralization of ECM in a dose-dependent manner. **e** Primary murine calvarial osteoblasts were treated with vehicle or 10 or 50 ng/ml IL-6 and 100 ng/ml sIL-6R in a time-course experiment (5, 15, and 30 min). Western blotting was performed using cell lysates. IL-6 significantly induced the phosphorylation of ERK, Akt2, and STAT3 in a dose-dependent manner. Representative data from at least three independent experiments are shown. Data are shown as mean ± SE. *n.s.* not significant; $*P < 0.05$; $**P < 0.001$; $***P < 0.001$

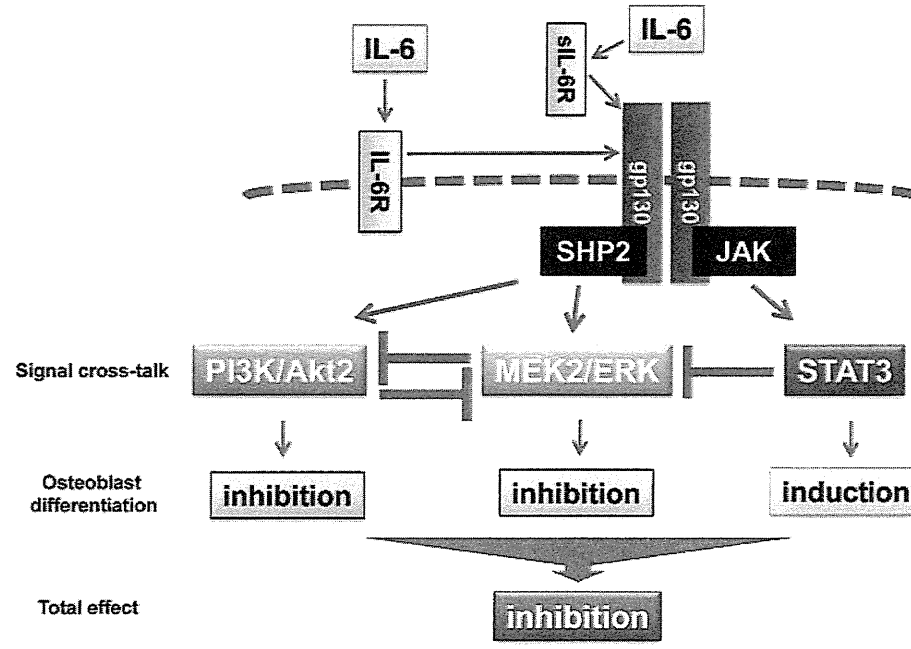

Fig. 9 Schematic presentation of signaling pathways involved in osteoblast differentiation induced by IL-6. IL-6-induced novel SHP2/MEK2/ERK and SHP2/PI3K/Akt2 signal crosstalk in osteoblastic cells; ERK and Akt signaling pathways, both of which are downstream of SHP2, negatively regulate each other reciprocally. On the other hand, the STAT3 signaling pathway negatively regulates the ERK signaling pathway. MEK2/ERK and PI3K/Akt2 have negative effects on osteoblast differentiation, whereas STAT3 has a positive effect. Overall, IL-6 inhibits osteoblast differentiation through MEK2 and Akt2 signaling pathways

SHP2/ERK and SHP2/Akt2 negatively affects osteoblast differentiation, whereas JAK/STAT3 positively affects it (Fig. 9). In other cells, it is often that simultaneous activation of the SHP2/ERK and JAK/STAT3 cascades generate opposing, or at least different signals. In osteoclasts, for example, SHP2/ERK activation inhibits osteoclastogenesis [53], whereas STAT3 is a pro-osteoclastic molecule after phosphorylation on serine727 [54]. In myeloid leukemic M1 cells, STAT3 induces differentiation in vitro [55], whereas the SHP2/ERK pathway promotes their proliferation [56]. These examples suggest that the integration of opposing activities transduced by more than one pathway could provide a biologically balanced state in the end, leaving availability to respond to another physiological situation. Indeed, Hirano and colleagues [57] have proposed a "signaling orchestration" model in a single cell, where the balance or interplay of simultaneously generated contradictory signals eventually determines the biological outcome. Thus, the inconsistent results regarding the effects of IL-6 on osteoblast differentiation in previous reports could be explained by which intracellular signaling pathway was predominantly activated in each study. The balance of three signaling pathways could be influenced by such conditions as the variety of cultured cells, the stage of cell differentiation, and the employed culture conditions.

To the best of our knowledge, this is the first report of signal crosstalk in which IL-6-induced ERK and Akt signaling pathways negatively regulated each other in cultured osteoblastic cells. In this study, however, cancellation of the negative effects of IL-6/sIL-6R on osteoblast differentiation by inhibitors was incomplete as compared to the absence of inhibitor (Figs. 5, 6). This might be because ERK, Akt and STAT3 are all critical pathways in osteoblast differentiation even in the absence of IL-6/sIL-6R, and even though one pathway is blocked, another pathway is enhanced by reciprocal regulation in the crosstalk between IL-6-activated signaling pathways (Fig. 9). Our results demonstrated that a STAT3 inhibitor significantly enhanced IL-6-induced activation of ERK and SHP2, but not of Akt (Fig. 4a). SHP2 could predominantly lead to the activation of the ERK signaling pathway as compared to Akt, and the enhanced signaling of ERK may restrain the enhancement of the Akt signaling pathway in a negative feedback manner.

The results obtained from the present study show that SHP2, MEK and PI3K inhibitors would be of potential use for the treatment of osteoporotic changes in RA patients. In particular, SHP2 inhibitors not only could inhibit the negative effect of IL-6-induced MEK/ERK and PI3K/Akt2 signaling, but also enhance the positive effect of IL-6-induced STAT3 signaling on osteoblast differentiation [37]. However, since a pro-inflammatory effect of STAT3 on synovitis has been reported [36, 58], selective inhibition of MEK2 and Akt2 signaling in osteoblasts may be more promising in order to avoid the enhancement of synovitis and consequent joint destruction.

In conclusion, our study provides new insights in the pathophysiology as well as potential treatment options for bone loss in RA, focusing on osteoblast differentiation in vitro. Our results demonstrated that IL-6 could inhibit osteoblast differentiation through MEK2/ERK and PI3K/Akt2 signaling pathways, both of which are SHP2-dependent downstream signaling pathways.

Conflict of interest All authors have no conflicts of interest.

References

1. Hashizume M, Mihara M (2011) The roles of interleukin-6 in the pathogenesis of rheumatoid arthritis. Arthritis 2011:765624
2. Ito A, Itoh Y, Sasaguri Y, Morimatsu M, Mori Y (1992) Effects of interleukin-6 on the metabolism of connective tissue components in rheumatoid synovial fibroblasts. Arthritis Rheum 35:1197–1201
3. Nishimoto N, Kishimoto T (2004) Inhibition of IL-6 for the treatment of inflammatory diseases. Curr Opin Pharmacol 4:386–391
4. De Benedetti F, Robbioni P, Massa M, Viola S, Albani S, Martini A (1992) Serum interleukin-6 levels and joint involvement in polyarticular and pauciarticular juvenile chronic arthritis. Clin Exp Rheumatol 10:493–498
5. De Benedetti F, Massa M, Pignatti P, Albani S, Novick D, Martini A (1994) Serum soluble interleukin 6 (IL-6) receptor and IL-6/soluble IL-6 receptor complex in systemic juvenile rheumatoid arthritis. J Clin Invest 93:2114–2119
6. Kotake S, Sato K, Kim KJ, Takahashi N, Udagawa N, Nakamura I, Yamaguchi A, Kishimoto T, Suda T, Kashiwazaki S (1996) Interleukin-6 and soluble interleukin-6 receptors in the synovial fluids from rheumatoid arthritis patients are responsible for osteoclast-like cell formation. J Bone Miner Res 11:88–95
7. Kwan Tat S, Padrines M, Theoleyre S, Heymann D, Fortun Y (2004) IL-6, RANKL, TNF-alpha/IL-1: interrelations in bone resorption pathophysiology. Cytokine Growth Factor Rev 15:49–60
8. Palmqvist P, Persson E, Conaway HH, Lerner UH (2002) IL-6, leukemia inhibitory factor, and oncostatin M stimulate bone resorption and regulate the expression of receptor activator of NF-kappa B ligand, osteoprotegerin, and receptor activator of NF-kappa B in mouse calvariae. J Immunol 169:3353–3362
9. Le Goff B, Blanchard F, Berthelot JM, Heymann D, Maugars Y (2010) Role for interleukin-6 in structural joint damage and systemic bone loss in rheumatoid arthritis. Joint Bone Spine 77:201–205
10. Hirano T, Matsuda T, Turner M, Miyasaka N, Buchan G, Tang B, Sato K, Shimizu M, Maini R, Feldmann M et al (1988) Excessive production of interleukin 6/B cell stimulatory factor-2 in rheumatoid arthritis. Eur J Immunol 18:1797–1801
11. Ohshima S, Saeki Y, Mima T, Sasai M, Nishioka K, Nomura S, Kopf M, Katada Y, Tanaka T, Suemura M, Kishimoto T (1998) Interleukin 6 plays a key role in the development of antigen-induced arthritis. Proc Natl Acad Sci USA 95:8222–8226
12. Dasgupta B, Corkill M, Kirkham B, Gibson T, Panayi G (1992) Serial estimation of interleukin 6 as a measure of systemic disease in rheumatoid arthritis. J Rheumatol 19:22–25
13. Poli V, Balena R, Fattori E, Markatos A, Yamamoto M, Tanaka H, Ciliberto G, Rodan GA, Costantini F (1994) Interleukin-6 deficient mice are protected from bone loss caused by estrogen depletion. EMBO J 13:1189–1196
14. Yang X, Ricciardi BF, Hernandez-Soria A, Shi Y, Pleshko Camacho N, Bostrom MP (2007) Callus mineralization and maturation are delayed during fracture healing in interleukin-6 knockout mice. Bone 41:928–936
15. Kopf M, Baumann H, Freer G, Freudenberg M, Lamers M, Kishimoto T, Zinkernagel R, Bluethmann H, Kohler G (1994) Impaired immune and acute-phase responses in interleukin-6-deficient mice. Nature 368:339–342
16. De Benedetti F, Rucci N, Del Fattore A, Peruzzi B, Paro R, Longo M, Vivarelli M, Muratori F, Berni S, Ballanti P, Ferrari S, Teti A (2006) Impaired skeletal development in interleukin-6-transgenic mice: a model for the impact of chronic inflammation on the growing skeletal system. Arthritis Rheum 54:3551–3563
17. Naka T, Nishimoto N, Kishimoto T (2002) The paradigm of IL-6: from basic science to medicine. Arthritis Res 4(Suppl 3):S233–S242
18. Wong PK, Campbell IK, Egan PJ, Ernst M, Wicks IP (2003) The role of the interleukin-6 family of cytokines in inflammatory arthritis and bone turnover. Arthritis Rheum 48:1177–1189
19. Garnero P, Thompson E, Woodworth T, Smolen JS (2010) Rapid and sustained improvement in bone and cartilage turnover markers with the anti-interleukin-6 receptor inhibitor tocilizumab plus methotrexate in rheumatoid arthritis patients with an inadequate response to methotrexate: results from a substudy of the multicenter double-blind, placebo-controlled trial of tocilizumab in inadequate responders to methotrexate alone. Arthritis Rheum 62:33–43
20. Franchimont N, Wertz S, Malaise M (2005) Interleukin-6: an osteotropic factor influencing bone formation? Bone 37:601–606
21. Li YP, Stashenko P (1992) Proinflammatory cytokines tumor necrosis factor-alpha and IL-6, but not IL-1, down-regulate the osteocalcin gene promoter. J Immunol 148:788–794
22. Peruzzi B, Cappariello A, Del Fattore A, Rucci N, De Benedetti F, Teti A (2012) c-Src and IL-6 inhibit osteoblast differentiation and integrate IGFBP5 signalling. Nat Commun 3:630
23. Hughes FJ, Howells GL (1993) Interleukin-6 inhibits bone formation in vitro. Bone Miner 21:21–28
24. Nishimura R, Moriyama K, Yasukawa K, Mundy GR, Yoneda T (1998) Combination of interleukin-6 and soluble interleukin-6 receptors induces differentiation and activation of JAK-STAT and MAP kinase pathways in MG-63 human osteoblastic cells. J Bone Miner Res 13:777–785
25. Taguchi Y, Yamamoto M, Yamate T, Lin SC, Mocharla H, DeTogni P, Nakayama N, Boyce BF, Abe E, Manolagas SC (1998) Interleukin-6-type cytokines stimulate mesenchymal progenitor differentiation toward the osteoblastic lineage. Proc Assoc Am Physicians 110:559–574
26. Ishihara K, Hirano T (2002) Molecular basis of the cell specificity of cytokine action. Biochim Biophys Acta 1592:281–296
27. Takahashi-Tezuka M, Yoshida Y, Fukada T, Ohtani T, Yamanaka Y, Nishida K, Nakajima K, Hibi M, Hirano T (1998) Gab1 acts as an adapter molecule linking the cytokine receptor gp130 to ERK mitogen-activated protein kinase. Mol Cell Biol 18:4109–4117
28. Hideshima T, Nakamura N, Chauhan D, Anderson KC (2001) Biologic sequelae of interleukin-6 induced PI3-K/Akt signaling in multiple myeloma. Oncogene 20:5991–6000
29. Tu Y, Gardner A, Lichtenstein A (2000) The phosphatidylinositol 3-kinase/AKT kinase pathway in multiple myeloma plasma cells: roles in cytokine-dependent survival and proliferative responses. Cancer Res 60:6763–6770
30. Chung TD, Yu JJ, Kong TA, Spiotto MT, Lin JM (2000) Interleukin-6 activates phosphatidylinositol-3 kinase, which inhibits apoptosis in human prostate cancer cell lines. Prostate 42:1–7
31. Qiu Y, Robinson D, Pretlow TG, Kung HJ (1998) Etk/Bmx, a tyrosine kinase with a pleckstrin-homology domain, is an effector of phosphatidylinositol 3′-kinase and is involved in interleukin 6-induced neuroendocrine differentiation of prostate cancer cells. Proc Natl Acad Sci USA 95:3644–3649
32. Chen RH, Chang MC, Su YH, Tsai YT, Kuo ML (1999) Interleukin-6 inhibits transforming growth factor-beta-induced apoptosis through the phosphatidylinositol 3-kinase/Akt and signal transducers and activators of transcription 3 pathways. J Biol Chem 274:23013–23019
33. Schmidt K, Schinke T, Haberland M, Priemel M, Schilling AF, Mueldner C, Rueger JM, Sock E, Wegner M, Amling M (2005) The high mobility group transcription factor Sox8 is a negative regulator of osteoblast differentiation. J Cell Biol 168:899–910

34. Ratisoontorn C, Seto ML, Broughton KM, Cunningham ML (2005) In vitro differentiation profile of osteoblasts derived from patients with Saethre-Chotzen syndrome. Bone 36:627–634
35. Hellmuth K, Grosskopf S, Lum CT, Wurtele M, Roder N, von Kries JP, Rosario M, Rademann J, Birchmeier W (2008) Specific inhibitors of the protein tyrosine phosphatase Shp2 identified by high-throughput docking. Proc Natl Acad Sci USA 105:7275–7280
36. Ernst M, Inglese M, Waring P, Campbell IK, Bao S, Clay FJ, Alexander WS, Wicks IP, Tarlinton DM, Novak U, Heath JK, Dunn AR (2001) Defective gp130-mediated signal transducer and activator of transcription (STAT) signaling results in degenerative joint disease, gastrointestinal ulceration, and failure of uterine implantation. J Exp Med 194:189–203
37. Itoh S, Udagawa N, Takahashi N, Yoshitake F, Narita H, Ebisu S, Ishihara K (2006) A critical role for interleukin-6 family-mediated Stat3 activation in osteoblast differentiation and bone formation. Bone 39:505–512
38. Sims NA (2004) Glycoprotein 130 regulates bone turnover and bone size by distinct downstream signaling pathways. J Clin Investig 113:379–389
39. Kawamura N, Kugimiya F, Oshima Y, Ohba S, Ikeda T et al (2007) Akt1 in osteoblasts and osteoclasts controls bone remodeling. PLoS One 2:e1058
40. Chen WS, Xu PZ, Gottlob K, Chen ML, Sokol K, Shiyanova T, Roninson I, Weng W, Suzuki R, Tobe K, Kadowaki T, Hay N (2001) Growth retardation and increased apoptosis in mice with homozygous disruption of the Akt1 gene. Genes Dev 15:2203–2208
41. Yang ZZ, Tschopp O, Hemmings-Mieszczak M, Feng J, Brodbeck D, Perentes E, Hemmings BA (2003) Protein kinase B alpha/Akt1 regulates placental development and fetal growth. J Biol Chem 278:32124–32131
42. Vandoorne K, Magland J, Plaks V, Sharir A, Zelzer E, Wehrli F, Hemmings BA, Harmelin A, Neeman M (2010) Bone vascularization and trabecular bone formation are mediated by PKB alpha/Akt1 in a gene-dosage-dependent manner: in vivo and ex vivo MRI. Magn Reson Med 64:54–64
43. Choi YH, Choi HJ, Lee KY, Oh JW (2012) Akt1 regulates phosphorylation and osteogenic activity of Dlx3. Biochem Biophys Res Commun 425:800–805
44. Mukherjee A, Rotwein P (2012) Selective signaling by Akt1 controls osteoblast differentiation and osteoblast-mediated osteoclast development. Mol Cell Biol 32:490–500
45. Mukherjee A, Wilson EM, Rotwein P (2010) Selective signaling by Akt2 promotes bone morphogenetic protein 2-mediated osteoblast differentiation. Mol Cell Biol 30:1018–1027
46. Ducy P, Desbois C, Boyce B, Pinero G, Story B, Dunstan C, Smith E, Bonadio J, Goldstein S, Gundberg C, Bradley A, Karsenty G (1996) Increased bone formation in osteocalcin-deficient mice. Nature 382:448–452
47. Higuchi C, Myoui A, Hashimoto N, Kuriyama K, Yoshioka K, Yoshikawa H, Itoh K (2002) Continuous inhibition of MAPK signaling promotes the early osteoblastic differentiation and mineralization of the extracellular matrix. J Bone Miner Res 17:1785–1794
48. Chaudhary LR, Avioli LV (2000) Extracellular-signal regulated kinase signaling pathway mediates downregulation of type I procollagen gene expression by FGF-2, PDGF-BB, and okadaic acid in osteoblastic cells. J Cell Biochem 76:354–359
49. Lin FH, Chang JB, Brigman BE (2011) Role of mitogen-activated protein kinase in osteoblast differentiation. J Orthop Res 29:204–210
50. Ge C, Xiao G, Jiang D, Franceschi RT (2007) Critical role of the extracellular signal-regulated kinase-MAPK pathway in osteoblast differentiation and skeletal development. J Cell Biol 176:709–718
51. Matsushita T, Chan YY, Kawanami A, Balmes G, Landreth GE, Murakami S (2009) Extracellular signal-regulated kinase 1 (ERK1) and ERK2 play essential roles in osteoblast differentiation and in supporting osteoclastogenesis. Mol Cell Biol 29:5843–5857
52. Schindeler A, Little DG (2006) Ras-MAPK signaling in osteogenic differentiation: friend or foe? J Bone Miner Res 21:1331–1338
53. Sims NA, Jenkins BJ, Quinn JM, Nakamura A, Glatt M, Gillespie MT, Ernst M, Martin TJ (2004) Glycoprotein 130 regulates bone turnover and bone size by distinct downstream signaling pathways. J Clin Invest 113:379–389
54. Duplomb L, Baud'huin M, Charrier C, Berreur M, Trichet V, Blanchard F, Heymann D (2008) Interleukin-6 inhibits receptor activator of nuclear factor kappaB ligand-induced osteoclastogenesis by diverting cells into the macrophage lineage: key role of Serine727 phosphorylation of signal transducer and activator of transcription 3. Endocrinology 149:3688–3697
55. Yamanaka Y, Nakajima K, Fukada T, Hibi M, Hirano T (1996) Differentiation and growth arrest signals are generated through the cytoplasmic region of gp130 that is essential for Stat3 activation. EMBO J 15:1557–1565
56. Nakajima K, Yamanaka Y, Nakae K, Kojima H, Ichiba M, Kiuchi N, Kitaoka T, Fukada T, Hibi M, Hirano T (1996) A central role for Stat3 in IL-6-induced regulation of growth and differentiation in M1 leukemia cells. EMBO J 15:3651–3658
57. Hirano T, Matsuda T, Nakajima K (1994) Signal transduction through gp130 that is shared among the receptors for the interleukin 6 related cytokine subfamily. Stem Cells 12:262–277
58. Krause A, Scaletta N, Ji JD, Ivashkiv LB (2002) Rheumatoid arthritis synoviocyte survival is dependent on Stat3. J Immunol 169:6610–6616

Bone 57 (2013) 429–436

Contents lists available at ScienceDirect

Bone

journal homepage: www.elsevier.com/locate/bone

Original Full Length Article

Novel sandwich ELISAs for rat DMP1: Age-related decrease of circulatory DMP1 levels in male rats

Sunao Sato [a], Jun Hashimoto [b], Yu Usami [c], Kaname Ohyama [d], Yukihiro Isogai [e], Yoshiaki Hagiwara [f], Nobuhiro Maruyama [f], Toshihisa Komori [g], Tatsuhiko Kuroda [e], Satoru Toyosawa [a,*]

[a] Department of Oral Pathology, Graduate School of Dentistry, Osaka University, Osaka, Japan
[b] Rheumatoid Center, National Hospital Organization, Osaka Minami Medical Center, Japan
[c] Clinical Laboratory, Osaka University Dental Hospital, Osaka, Japan
[d] Department of Environmental and Pharmaceutical Sciences, Graduate School of Biomedical Sciences, Nagasaki University, Nagasaki, Japan
[e] Project for Bone Metabolic Diseases, Pharmaceuticals Sales Division, Asahi Kasei Pharma Corporation, Tokyo, Japan
[f] Immuno-Biological Laboratories Co., Ltd, Gunma, Japan
[g] Department of Developmental and Reconstructive Medicine, Nagasaki University Graduate School of Biomedical Sciences, Nagasaki, Japan

ARTICLE INFO

Article history:
Received 24 May 2013
Revised 14 September 2013
Accepted 20 September 2013
Available online 26 September 2013

Edited by: Toshio Matsumoto

Keywords:
Dentin matrix protein 1 (DMP1)
Enzyme-linked immunosorbent assay (ELISA)
Osteocyte
Bone turnover
Aging

ABSTRACT

Dentin matrix protein 1 (DMP1), a noncollagenous bone matrix protein produced by osteocytes, regulates matrix mineralization and phosphate homeostasis. The lack of a precise assay for circulating DMP1 levels impairs further investigation of the protein's biological significance. Because full-length precursor DMP1 is cleaved into NH_2- and COOH-terminal fragments during the secretory process, we developed two new sandwich ELISAs for the NH_2- and COOH-terminal fragments of rat DMP1. One of these ELISAs, ELISA 1–2, is based on two affinity-purified polyclonal antibodies against the DMP1-1 and DMP1-2 peptides of the NH_2-terminal fragment, whereas the other, ELISA 4–3, is based on two affinity-purified polyclonal antibodies against the DMP1-3 and DMP1-4 peptides of the COOH-terminal fragment. The polyclonal antibodies were characterized in immunohistochemical and liquid chromatography–electrospray ionization tandem mass spectrometry (LC–MS/MS) studies. Immunohistochemical analyses of rat bone using these polyclonal antibodies revealed DMP1 immunoreactivity in osteocytes and pericanalicular matrix, consistent with the previously reported osteocyte-specific expression of DMP1. LC–MS/MS analyses of rat plasma-derived immunoreactive products affinity-extracted with these antibodies revealed the presence of DMP1 in circulating blood. The ELISAs established with these antibodies met accepted standards for reproducibility, repeatability, precision, and accuracy. Circulating DMP1 and levels of other biochemical markers (osteocalcin, Trap5b, Dkk-1, and SOST) were measured in 2-, 4-, 8-, 12-, 18-, 24-, 72-, and 96-week-old Wistar male rats. Circulating DMP1 levels determined by ELISAs 1–2 and 4–3 significantly decreased with age. During rapid skeletal growth (2–12 weeks), DMP1 levels measured by ELISA 4–3 were over three times higher than those measured by ELISA 1–2; however, DMP1 levels in old animals (72 and 96 weeks) were almost the same when measured by either ELISA. DMP1 levels determined by both ELISAs were most highly positively correlated with the level of Dkk-1, second most highly correlated with the level of osteocalcin, and less highly correlated with the levels of Trap5b and SOST. These novel sandwich ELISAs for rat DMP1 are highly specific and allow precise measurements of circulating DMP1, which may be a new biochemical marker for osteocyte-mediated bone turnover.

Introduction

Dentin matrix protein 1 (DMP1), which is expressed in osteocytes [1], is a member of the SIBLING (Small Integrin-Binding Ligand, N-linked Glycoprotein) family of genetically related non-collagenous matrix proteins in mineralized tissues [2]. DMP1 contains an unusually large number of acidic domains; because of its highly acidic nature, DMP1 can bind to calcium, thereby regulating matrix mineralization [3]. Protein chemistry analysis has shown that full-length DMP1 is synthesized as a precursor that is cleaved into NH_2-terminal 37-kDa and COOH-terminal 57-kDa fragments [4]; however, a full-length form (105 kDa) of DMP1 has also been detected in bone and dentin, albeit at considerably lower levels [5]. DMP1-null mice exhibit hypophosphatemia, leading to the discovery of DMP1 mutations associated with autosomal-recessive hypophosphatemic rickets (ARHR) in humans [6,7]. Both DMP1-null mice and individuals with ARHR exhibit elevated serum FGF23, which causes increased renal phosphate wasting

* Corresponding author at: Department of Oral Pathology, Graduate School of Dentistry, Osaka University, 1-8 Yamadaoka, Suita, Osaka 565-0871, Japan. Fax: +81 6 6879 289.
E-mail address: toyosawa@dent.osaka-u.ac.jp (S. Toyosawa).

8756-3282/$ – see front matter © 2013 Elsevier Inc. All rights reserved.
http://dx.doi.org/10.1016/j.bone.2013.09.013

leading to hypophosphatemia. These findings indicate that regulation of matrix mineralization by DMP1 is coupled to renal phosphate homeostasis via FGF23 production by osteocytes.

Cellular and extracellular components of the skeletal tissue have been used to develop the biochemical markers that specifically reflect either bone formation or bone resorption [8]. These markers may be classified according to the biological compartment to which they belong, parameters of cellular (osteoblast and osteoclast) activity, and components released during bone formation and breakdown of the bone matrix. Osteocytes, which are the most abundant and longest-living cells in the adult skeleton, have recently been found to control bone remodeling through regulation of both osteoclast and osteoblast activity, and also to function as endocrine cells [9]. The targeted ablation of osteocytes in cortical bone generated osteoclast activation [10]. On the other hands, osteocyte as a mechanosensory cells coordinates the osteoblatic activity to mechanical force by downregulating sclerostin [11]. Further, osteocyte as an endocrine cell produces FGF-23, which leads to phosphate excretion in the kidney, thereby controls circulation phosphate [6]. These findings indicated that osteocyte viability and activity clearly plays a significant role in the maintenance of bone homeostasis and integrity. In fact, osteocyte density was decreased in the vertebral fracture patients than in the controls [12], and osteocyte lacunar density was decreased with an increase in bony porosity and microcrack density [13]. Until now, these osteocytic changes have been studied with histomorphometric analysis and three-dimensional imaging analyses of bone samples [14]. However, these methods give information on limited areas of whole skeletal bone and are not the noninvasive techniques suitable for routine analyses. Given that DMP1 is produced predominantly in osteocytes, whereas other bone matrix proteins (including osteopontin, osteocalcin, and bone sialoprotein) are produced in osteoblasts [1,15–17], circulating DMP1 represents a candidate biochemical marker for osteocyte activity as well as bone mineralization.

To assess the potential utility of DMP1 as a biochemical marker of bone metabolism under physiological and pathological conditions, it would be very useful to develop precise assays for measurement of DMP1 levels in circulating blood, and to use these assays to evaluate the normal range of circulating DMP1 levels. In this study, we quantitatively determined the normal range of circulating DMP1 levels in rats of various ages (2–96 weeks) using newly development sandwich ELISAs, and analyzed the relationship between the levels of DMP1 and other biochemical markers of bone metabolism.

Materials and methods

Production of polyclonal antibodies against rat DMP1

Peptides encoding rat DMP1 residues 90–111 (DMP1-1: SGDDTFG DEDNGPGPEERQWGG), 148–164 (DMP1-2: HHSDEADSRPEAGDSTQ), 247–261 (DMP1-3: FRRSRVSEEDDRGEL), and 275–293 (DMP1-4: EDFRSKEESRSETQEDTAE) were prepared, with cysteines affixed NH_2-terminally to DMP1-1, -3, and -4 and COOH-terminally to DMP1-2 (American Peptide Company, Sunnyvale, CA, USA) (Fig. 1). The cysteinyl peptides were conjugated to bovine thyroglobulin and dialyzed, and the coupled peptides were then mixed with Freund's complete adjuvant (DIFCO, Lawrence, KS, USA) and injected subcutaneously into two Japanese white rabbits (approximately 100 μg per animal). Eight subcutaneous booster injections with Freund's incomplete adjuvant (DIFCO) were also performed (approximately 100 μg per animal). Anti-rat DMP1 peptide antisera were affinity-purified by acetic acid elution from a peptide-conjugated Activated Thiol Sepharose4B (GE Healthcare Life Sciences, Pittsburgh, PA, USA). Affinity-purified rabbit polyclonal antibodies against rat DMP1 peptides were used for immunohistochemistry, immunoaffinity chromatography, and rat DMP1 ELISAs. All animal procedures in this study were approved by Osaka University Graduate School of Dentistry Intramural Animal Use and Care Committee.

Immunohistochemistry of rat bone

One-week-old Wistar rats (n = 3) were fixed by transcardiac perfusion of 4% paraformaldehyde under general anesthesia. Tibia samples were immersed in fixative overnight at 4 °C and demineralized with buffered 10% EDTA for 7 days at 4 °C. The samples were embedded in paraffin, and serial sections (5 μm thick) were prepared and mounted onto silane-coated slides.

Fig. 1. Amino-acid sequence of rat DMP1. The sequences of peptides DMP1-1, -2, -3, and -4, used for immunization, are shown with a shaded background and underlining. The DMP1 peptides identified by LC-MS/MS analyses of plasma-derived immunoreactive products affinity-purified with antibodies against DMP1-1 or DMP1-3 are shown in bold type. Arrowheads indicated the cleavage sites between the NH_2-terminal 37-kDa and COOH-terminal 57-kDa fragments [4].

Immunohistochemical staining was performed using the streptavidin-biotin complex (sABC) peroxidase method and the anti-rabbit sABC system from Dako (Glostrup, Denmark). Primary rabbit polyclonal antibodies against DMP1-1, -2, -3, and -4 were used. Tissue sections were treated with trypsin to facilitate antigen exposure for immunostaining. Sections were lightly counterstained with hematoxylin. As negative controls, rabbit serum IgG (Dako) was used as the primary antibody, yielding uniformly negative results.

Peptide sequencing of immunoreactive products with antibodies for DMP1

Each immunoreactive product was extracted from 20 mL EDTA plasma of 1-month-old male Wistar rats by immunoaffinity chromatography, using antibodies against the DMP1-1 or DMP1-3 peptides. The immunoreactive product was condensed by freeze-dehydration and used for peptide sequencing. Digestion of these products followed an established methodology [18]. Briefly, the products (approximately 200 ng/100 μL) were reduced with dithiothreitol (Wako Pure Chemical, Osaka, Japan) and then alkylated with iodoacetamide (Wako Pure Chemical). Subsequently, the samples were digested with trypsin (Promega, Madison, MI, USA) overnight at 37 °C.

The resulting peptide mixture was analyzed on a liquid chromatography–electrospray ionization tandem mass spectrometer (LC-MS/MS) (LTQ XL; Thermo Fisher Scientific, Waltham, MA, USA) equipped with a custom nano-LC system consisting of a Shimadzu LC pump (Shimadzu, Kyoto, Japan) with LC flow splitter (Dionex, Idstein, Germany) and an HCT PAL autosampler (CTC Analytics, Zwingen, Germany). The sample was loaded onto a nano-precolumn (300 μm i.d. × 5.0 mm, L-C-18; Chemicals and Evaluation and Research Institute, Tokyo, Japan) in the injection loop and washed using 0.1% trifluoroacetic acid in 2% acetonitrile. Peptides were separated using a nano-HPLC column (75 μm i.d. × 15 cm, Acclaim PepMap100C18, 3 μm, Dionex) and ion-sprayed into the MS at a spray voltage of 1.5 kV. The mass spectrometer was configured to acquire data by progressing from a full scan of the sample to three tandem MS scans of the three precursor masses (m/z 730.2 corresponding to YQNTESESSEER; m/z 1000.6 corresponding to SEESKGDHEPTSTQDSDDSQDVEFSSR; m/z 746.7 corresponding to SKEESNSTGSTSSSEEDNHPK) (Fig. 1) as determined in real time by the Xcalibur® software (Thermo Fisher Scientific). The MS/MS spectra obtained from these precursor ions were searched against the rat subdatabase of the public non-redundant protein database of the International Protein Index, version 3.87, provided by The European Bioinformatics Institute.

Generation of recombinant rat DMP1

Glutathione-S-transferase (GST)-fused rat DMP1 was created by subcloning a fragment of the coding region of the rat DMP1 cDNA (excluding the signal peptide) in an *E. coli* expression system, described previously [1]. Purified recombinant rat DMP1 was kept at −20 °C prior to use.

Development of sandwich ELISA for the detection of rat DMP1

The sandwich ELISA system for the detection of rat DMP1 was constructed by Immuno-Biological Laboratories Co., Ltd. (Gunma, Japan). Four affinity-purified antibodies were immobilized on the 96-well microtiter-plate, and conjugated horseradish peroxidase (HRP) (Toyobo, Osaka, Japan) was used to test different combinations of capture and detection antibodies in sandwich ELISA. In the assay, 100 μL of recombinant rat DMP1 or rat blood samples were used. The assay procedure was as follows. Microtiter plates (96 wells) were coated by addition of 100 μl of 100 mmol/L carbonate buffer (pH 9.5) containing 1.0 μg of purified antibody to each well, followed by incubation overnight at 4 °C. The plates were washed with PBS containing 0.05% Tween-20 (PBS-T), and then blocked overnight at 4 °C with 200 μL per well of 1% (w/v) bovine serum albumin (BSA) in PBS containing 0.05% NaN_3. Following two washes with PBS-T, test samples and recombinant rat DMP1 (as a standard) were added in duplicate to the wells of the coated microtiter plate and incubated for 1 h at 37 °C. After four washes with PBS-T, 100 μL of HRP-conjugated antibody was added to each well, and the samples were incubated for 30 min at 4 °C. The wells were washed five times with PBS-T, and then 100 μL of tetramethyl benzidine solution (Immuno-Biological Laboratories) was added to each well as a substrate, followed by incubation in the dark for 30 min at room temperature. The reaction was terminated by addition of 100 μL of 0.5 mol/L H_2SO_4. Absorbance of the solution was measured at 450 nm using an ELISA reader (iMark; Bio-Rad Laboratories, CA, USA). Finally the concentrations of unknown samples were calculated based on the recombinant rat DMP1 standard curve.

ELISA validation

In order to assess the intra- and inter-assay precision for the ELISA, three quality control (QC) samples were established covering the high, middle, and low range of the standard curves. Intra-assay precision was determined by 24 repeated measurements of each QC sample in a single plate, and inter-assay precision was determined by assessing each QC sample across six different plates in quintuplicate wells. Moreover, to assess the recovery rate in blood, different concentrations of recombinant rat DMP1 were added to samples and measured, and the recovery rate was calculated based on the difference between the measured and theoretical concentrations. The sensitivity of this kit was determined based on the guidelines provided by the National Committee for Clinical Laboratory Standards (NCCLS) Evaluation Protocols.

Other biochemical markers of bone metabolism

Plasma osteocalcin, a marker of bone formation, was measured by ELISA using antibodies raised against the middle region of human osteocalcin (Rat-MID™ Osteocalcin EIA; Immunodiagnostic Systems, Fountain Hills, AZ, USA). Plasma tartrate-resistant acid phosphatase isoenzyme 5b (TRAP5b), an osteoclast-specific enzyme, was measured by ELISA using a capture antibody raised against recombinant mouse TRAP5b (RatTRAP™; Immunodiagnostic Systems). Plasma Dickkopf-1 (Dkk-1), an osteocyte-expressed soluble inhibitor of the Wnt signaling pathway, was measured by ELISA using a capture antibody raised against Dkk-1 (Dkk-1 [rat], EIA kit; Enzo Life Sciences, Farmingdale, NY, USA). Plasma sclerostin (SOST), an osteocyte-expressed negative regulator of bone formation, was measured by ELISA using a capture antibody raised against recombinant mouse SOST (Quantikine ELISA Mouse/Rat SOST Immunoassay; R&D Systems, Minneapolis, MN, USA).

Study subjects

For the determination of the levels of DMP1 and the other biochemical markers as a function of the age of the animal, blood samples (EDTA plasma) were collected from male Wistar rats at 2, 4, 8, 12, 18, 24, 72, and 96 weeks of age (n = 43).

Statistical analysis

All statistical analyses were performed using JMP (Japanese version 10.0.0, SAS Institute, Cary, NC, USA). All comparisons of results from different age groups were performed by ANOVA and subsequent Tukey–Kramer test. All bar diagrams represent mean values, and error bars represent standard deviations (SDs). The correlations were calculated using the Pearson correlation coefficient. Statistical significance was defined as $p < 0.05$.

Results

Immunohistochemistry of DMP1 in rat bone

To characterize the polyclonal antibodies against the rat DMP1-1, DMP1-2, DMP1-3, and DMP1-4 peptides, we performed immunohistochemistry on rat bones using these antibodies. Analyses using anti-DMP1-1 or -DMP1-2 antibodies revealed immunoreactivity in the osteocytes and their surrounding bone matrix (Figs. 2a, b). By contrast, analyses using anti-DMP1-3 or -DMP1-4 antibodies revealed immunoreactivity in the pericanalicular matrix rather than in osteocytes (Figs. 2c, d). All these antibodies revealed no immunoreactivity in osteoblasts (Figs. 2a–d). These patterns of immunoreactivity in osteocytes and osteocyte-related matrix were consistent with the previously reported osteocytic expression of DMP1. From these observations, we concluded that the polyclonal antibodies correctly recognize local DMP1 in the bone.

Identification of circulating DMP1 in blood

To confirm the presence of DMP1 in circulating blood, we extracted immunoreactive products from rat plasma by affinity chromatography using antibodies against DMP1-1 or DMP1-3, and analyzed these products by LC-MS/MS. The LC-MS spectra of the immunoreactive products affinity-extracted with the polyclonal antibody against DMP1-1 (which recognizes for NH_2-terminal fragments of DMP1) revealed the YQNTESESSEER, SEESKGDHEPTSTQDSDDSQDVEFSSR, and SKEESNSTGSTSSSEEDNHPK peptides of rat DMP1 (Fig. 1). Likewise, the LC-MS spectra of the immunoreactive products affinity-extracted with the polyclonal antibody against DMP1-3 (which recognizes COOH-terminal fragments of DMP1) revealed the same three peptides. These findings confirmed that DMP1 was present in circulating blood, and that these antibodies could detect the circulating DMP1.

Development and characteristics of rat DMP1 immunoassay

Previous studies demonstrated that cleavages at four sites within DMP1 produce NH_2- and COOH-terminal fragments, with only a small amount of DMP1 remaining uncleaved [4,5]. In fact, ELISA using pairs of antibodies that recognized uncleaved DMP1 did not have sufficient sensitivity to detect circulating DMP1 (data not shown). We selected pairs of antibodies that recognized either the NH_2- or COOH-terminal fragments. In sandwich ELISA 1–2, polyclonal antibodies against the DMP1-1 and DMP1-2 peptides of the NH_2-terminal fragment were used, with anti-DMP1-1 as the capture antibody and HRP-conjugated anti-DMP1-2 as the detection antibody (Fig. 1). In sandwich ELISA 4–3, polyclonal antibodies against the DMP1-3 and DMP1-4 peptides of the COOH-terminal fragment were used, with anti-DMP1-4 as the capture antibody and HRP-conjugated anti-DMP1-3 as the detection antibody (Fig. 1). Dilutions of recombinant rat DMP1 were used for the standard curve.

The sensitivity of the assay was calculated to be 4.04 pg/mL for ELISA 1–2 and 2.51 pg/mL for ELISA 4–3 using NCCLS methods. The precision was determined using three spiked QC samples (high, middle, and low). Intra-assay variations ($n = 24$) were less than 5.7% for ELISA 1–2 (Table 1) and less than 8.6% for ELISA 4–3 (Table 2), and inter-assay variations ($n = 6$) were less than 6.3% for ELISA 1–2 (Table 1) and less than 8.2% for ELISA 4–3 (Table 2). Blood samples, collected either as EDTA plasma or serum, exhibited no appreciable differences in the detectable concentration of immunoreactive DMP1 (data not shown). Dilution

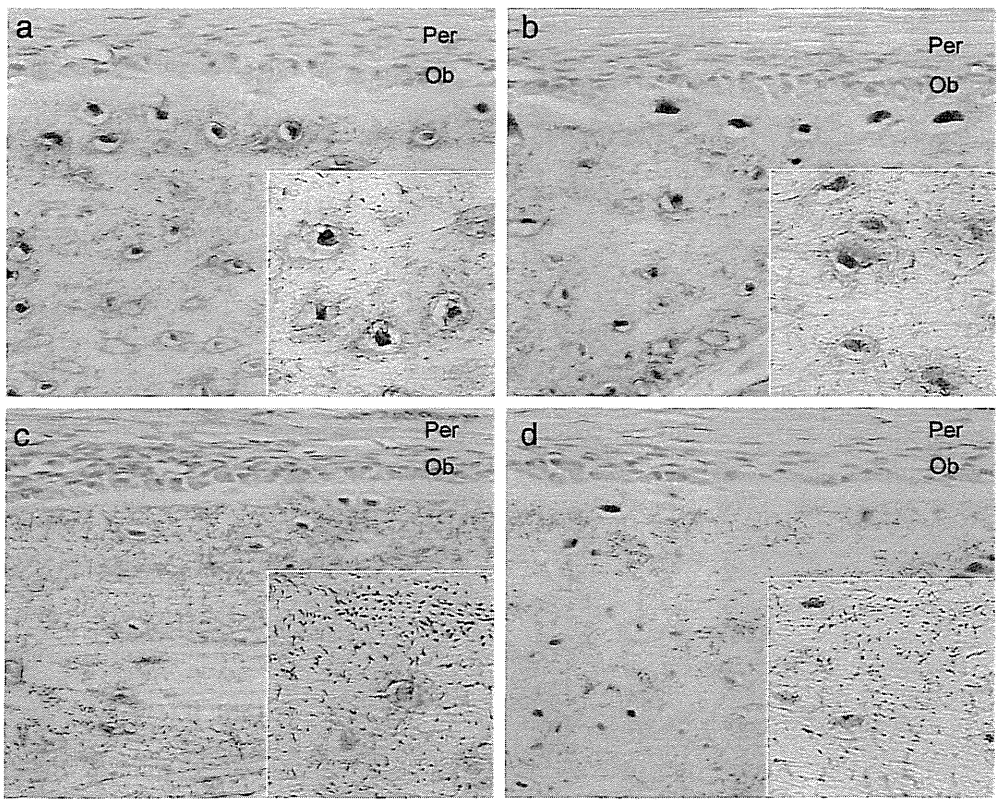

Fig. 2. Immunohistochemistry of local DMP1 in rat bone. (a) Immunostaining with antibody against DMP1-1 was seen in osteocytes and their surrounding bone matrix. (b) Immunostaining with antibody against DMP1-2 was seen in osteocytes and their surrounding bone matrix. (c) Immunostaining with antibody against DMP1-3 was seen in pericanalicular matrix rather than in osteocytes. (d) Immunostaining with antibody against DMP1-4 was seen in pericanalicular matrix rather than in osteocytes. (a)–(d) Immunostaining with antibodies against DMP1-1, 2, 3, 4 was not seen in osteoblasts. Insets in (a)–(d) show a higher magnification of osteocytes. Ob; osteoblast, Per; periosteum. Counterstaining was performed with hematoxylin. Original magnification, ×400. (Inset) Original magnification, ×700.

Table 1
Intra- and interassay precision of three control rat plasma samples in DMP1 ELISA 1-2.

	Intraassay variation (n = 24)		Interassay variation (n = 6)	
	Mean ± SD		Mean ± SD	
Sample	(pg/mL)	CV (%)	(pg/mL)	CV (%)
Low control	81.5 ± 3.74	4.6	83.8 ± 5.31	6.3
Medium control	306.5 ± 13.64	4.5	307.0 ± 13.29	4.3
High control	1049.1 ± 59.39	5.7	1081.3 ± 36.36	3.4

n: number of determinations
SD: standard deviation
CV: coefficient of variation

Table 2
Intra- and interassay precision of three control rat plasma samples in DMP1 ELISA 4-3.

	Intraassay variation (n = 24)		Interassay variation (n = 6)	
	Mean ± SD		Mean ± SD	
Sample	(pg/mL)	CV (%)	(pg/mL)	CV (%)
Low control	90.1 ± 7.78	8.6	87.0 ± 7.13	8.2
Medium control	306.0 ± 18.75	6.1	318.6 ± 23.57	7.4
High control	1045.7 ± 68.87	6.6	1121.5 ± 50.90	4.5

n: number of determinations
SD: standard deviation
CV: coefficient of variation

Table 3
Recovery of rat DMP1 in ELISA 1–2.

Sample no.	Theoretical value (pg/mL)	Measured value (pg/mL)	Recovery (%)
Rat EDTA plasma			
Sample 1	537.7	486.8	90.5
Sample 2	459.6	423.7	92.2
Sample 3	420.5	386.0	91.8
Rat serum			
Sample 4	959.3	889.3	92.7
Sample 5	881.2	838.8	95.2
Sample 6	842.1	763.5	90.7

Table 4
Recovery of rat DMP1 in ELISA 4-3.

Sample no.	Theoretical value (pg/mL)	Measured value (pg/mL)	Recovery (%)
Rat EDTA plasma			
Sample 1	1342.8	1303.4	97.1
Sample 2	1264.7	1217.1	96.2
Sample 3	1225.7	1182.5	96.5
Rat serum			
Sample 4	2179.6	2126.4	97.6
Sample 5	2101.5	2041.7	97.2
Sample 6	2062.4	2002.2	97.1

linearity was determined from three plasma samples (from 12, 18, and 96-week-old rats) in triplicate after serial dilution (ranging from 1:16 to 1:1024) with assay buffer; graphs of these were approximately parallel to the standard curve (Fig. 3). Plasma samples from three normal rats were incubated at 4 °C for 24 h or 37 °C for 1 h, and the DMP1 levels in these plasma samples were compared with those of the same plasma samples stored at −80 °C. In ELISA 1–2, the DMP1 concentration in plasma of 12-week-old rats incubated at 4 °C and 37 °C was 97.7 ± 20.9% (mean ± SD) and 99.0 ± 21.5% (mean ± SD) of the concentration in control plasma stored at −80 °C. In ELISA 4–3, the DMP1 concentration in plasma of 12-week-old rats incubated at 4 °C and 37 °C was 94.5 ± 21.3% (mean ± SD) and 91.3 ± 18.5% (mean ± SD) of the concentration in control plasma stored at −80 °C.

Studies in which recombinant rat DMP1 was added to 40- or 80-fold diluted rat EDTA plasma, yielded recoveries of 90.5–92.2% in ELISA 1–2 (Table 3) and 96.2–97.1% in ELISA 4–3 (Table 4). Studies in which recombinant rat DMP1 was added to 40- or 80-fold diluted rat serum, yielded recoveries of 90.7–95.2% in ELISA 1–2 (Table 3) and of 97.1–97.6% in ELISA 4–3 (Table 4).

Age-associated decrease of circulating DMP1 levels in male rats

We determined reference levels for circulating DMP1 in normal male rats of various ages (2–96 weeks). Both ELISA 1–2 and ELISA 4–3 showed that circulating DMP1 concentrations significanlly decrease with age (Fig. 4). During rapid skeletal growth (2–12 weeks), mean DMP1 values measured by ELISA 4–3 were over three times higher than those measured by ELISA 1–2. However, mean DMP1 values in old animals (72 and 96 weeks) were almost the same when measured by either ELISA.

Correlations between levels of DMP1 and other biochemical markers

We also measured the levels of the other biochemical markers of bone metabolism in normal male rats of various ages (2–96 weeks) (Fig. 5) and assessed the correlations between the levels of DMP1 and these other markers. Both osteocalcin and Dkk-1 levels tended to decrease with age. Both Trap5b and SOST levels were increased at 8 weeks and decreased after 12 weeks. Among all bone markers,

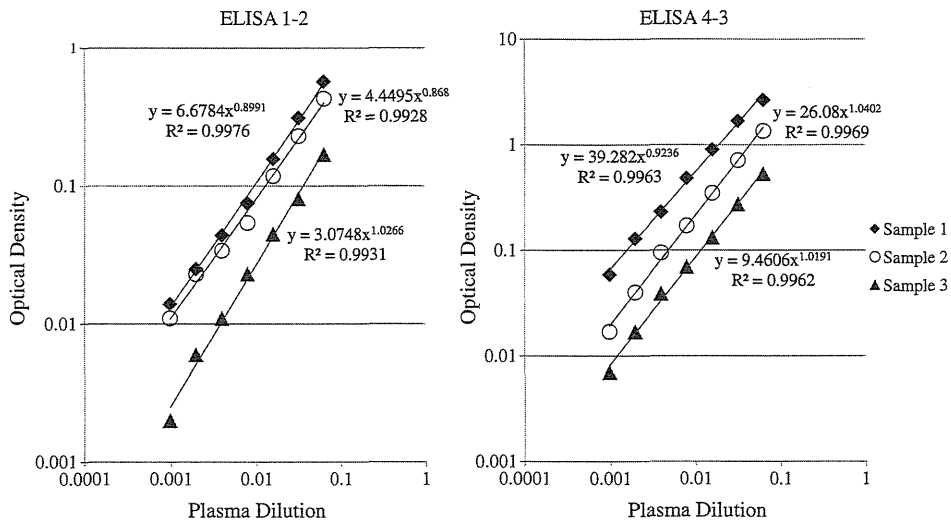

Fig. 3. Linearity of dilution studied in rat DMP1 ELISA assays. Each data point of ELISA 1–2 (left) or ELISA 4–3 (right) represents the mean of three separate measurements. Linear regression equations, together with the squares of the correlation coefficients (R^2), are shown.

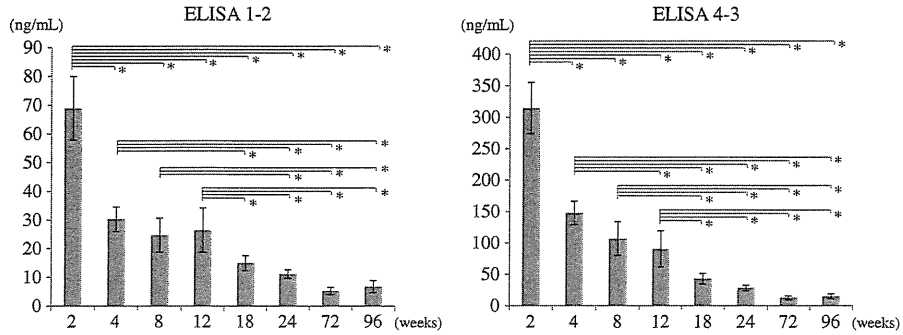

Fig. 4. DMP1 concentrations in plasma from male rats of various ages. Circulating DMP1 concentrations were evaluated in 2- (n = 5), 4- (n = 5), 8- (n = 6), 12- (n = 6), 18- (n = 6), 24- (n = 5), 72- (n = 5), and 96- (n = 5) week-old male Wistar rats by DMP1 ELISA 1–2 (left) and ELISA 4–3 (right). Values are expressed as means ± SD of DMP1 concentrations at each age. All comparisons between results from different age groups are shown, with $p < 0.05$ indicating a significant difference (*).

DMP1 levels measured by ELISA 1–2 had the highest positive correlation with DMP1 levels measured by ELISA 4–3 (Table 5). Among the other biochemical markers, DMP1 levels measured by both ELISAs 1–2 and 4–3 had the highest positive correlation with levels of Dkk-1, and the second highest positive correlation with the levels of osteocalcin; DMP1 levels were less highly correlated with the levels of Trap5b and SOST (Table 5).

Discussion

DMP1 is a noncollagenous bone matrix proteins produced by osteocytes [1]. Due to its highly acidic nature, DMP1 can bind to calcium, thereby regulating matrix mineralization [3]. Observations made in DMP1-null mice and humans with DMP1 mutations associated with autosomal-recessive hypophosphatemic rickets (ARHR) have shown that impairment of DMP1 results in elevated serum FGF23, which regulates phosphate homeostasis, and in pathological changes of bone mineralization [6,7]. However, the biological function of DMP1 is not yet fully understood. Considering that DMP1 is predominantly produced in osteocytes, whereas other bone matrix proteins such as osteocalcin, osteopontin, and bone sialoprotein are produced in osteoblasts [1,15–17], DMP1 in circulating blood is a candidate marker for osteocyte activity. To investigate the biological significance of DMP1, we developed new sandwich ELISAs for measuring rat DMP1 and used these assays to monitor age-related changes in circulating DMP1 levels. In addition, we analyzed the correlations between levels of DMP1 and other biochemical markers of bone metabolism.

We developed sandwich ELISAs for rat DMP1 using two pairs of polyclonal antibodies with high affinity to rat DMP1. These polyclonal antibodies were characterized by immunohistochemical and LC-MS/MS studies. In immunohistochemical analyses of rat bone using these antibodies, we observed immunoreactivity in osteocytes and pericanalicular matrix, as previously reported. LC-MS/MS analyses of rat plasma-derived immunoreactive products affinity-extracted with our polyclonal antibodies revealed the presence of DMP1 in circulating blood. It is generally accepted that a small fraction of bone matrix protein, such as osteocalcin, is released from the bone into the circulation, where it can be detected by immunoassay [8]. Similarly, a small fraction

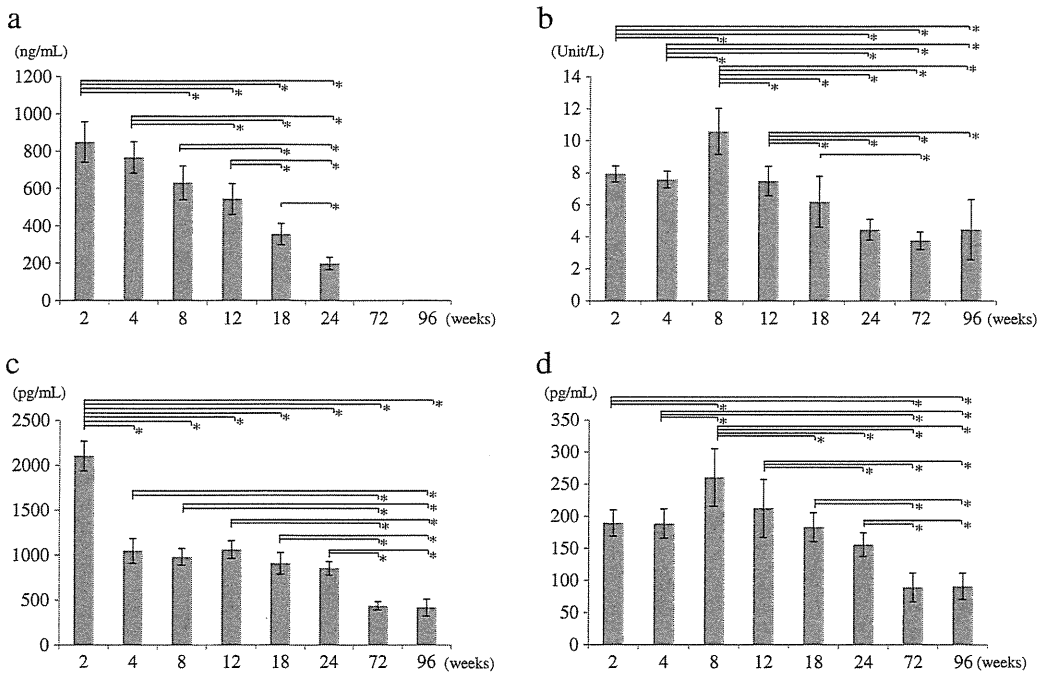

Fig. 5. Plasma levels of other biochemical markers. Plasma levels of the other biochemical markers were evaluated in 2- (n = 5), 4- (n = 5), 8- (n = 6), 12- (n = 6), 18- (n = 6), 24- (n = 5), 72- (n = 5), and 96- (n = 5) week-old male Wistar rats. Values are expressed as means ± SD of plasma levels of the indicated biochemical markers at each age. All comparisons between results from different age groups are shown, with $p < 0.05$ indicating a significant difference (*). (a) Osteocalcin levels. The levels at 72 and 96 weeks were off the register because of the low level of plasma osteocalcin. (b) Trap5b levels. (c) Dkk-1 levels. (d) SOST levels.

Table 5
Correlations between levels of DMP1 and other biochemical markers.

DMP1 levels	vs.	Other bone markers	R	p
DMP1 by ELISA 1–2		DMP1 by ELISA 4–3	0.986	<0.001
DMP1 by ELISA 1–2		TRAP	0.515	<0.001
DMP1 by ELISA 1–2		Osteocalcin	0.800	<0.001
DMP1 by ELISA 1–2		Dkk-1	0.921	<0.001
DMP1 by ELISA 1–2		SOST	0.453	0.002
DMP1 by ELISA 4–3		TRAP	0.512	<0.001
DMP1 by ELISA 4–3		Osteocalcin	0.833	<0.001
DMP1 by ELISA 4–3		Dkk-1	0.910	<0.001
DMP1 by ELISA 4–3		SOST	0.417	0.005

of DMP1, synthesized by osteocytes in the bone, is likely to be released into the blood circulation. Taken together, the novel sandwich ELISAs established with our polyclonal antibodies, which can detect both circulating DMP1 and local bone DMP1, can accurately detect circulating DMP1, which reflects local bone conditions. Further, the results of recovery of recombinant DMP1 and dilution of plasma samples strongly suggested that both ELISA 1–2 and ELISA 4–3 recognized the circulating DMP1 and the standard with similar affinities. The sensitivity of these assays was sufficient to detect circulating DMP1 in healthy male rats of various ages.

Theoretically, ELISAs 1–2 and 4–3 could both detect uncleaved DMP1 as well as the NH_2- and COOH-terminal fragments, respectively. However, protein-chemistry analysis has shown that full-length DMP1 is a precursor that is cleaved into NH_2-terminal 37-kDa and COOH-terminal 57-kDa fragments [4]. Furthermore, it is nearly impossible to detect and extract full-length DMP1 from bone matrix because of the very small quantity of full-length protein in the bone [5]. Indeed, as already noted, ELISAs using pairs of antibodies that recognized uncleaved DMP1 did not have sufficient sensitivity to detect circulating DMP1 (data not shown). Therefore, we conclude that ELISA 1–2 predominantly detects circulating NH_2-terminal fragments of DMP1, and ELISA 4–3 predominantly detects circulating COOH-terminal fragments of DMP1.

Immunoassays using ELISAs 1–2 and 4–3 revealed the same general tendency of reduction in circulating DMP1 levels as a function of age, but there were some differences in measurements obtained using the two ELISAs. The mean values for circulating COOH-terminal DMP1 during rapid skeletal growth (2–12 weeks) were over three times higher than those of circulating NH_2-terminal DMP1. On the other hands, the means of the COOH-terminal and NH_2-terminal DMP1 in samples from older animals (72 and 96 weeks) were almost the same between the two ELISAs. These findings indicated that higher levels of COOH-terminal DMP1 are released from bone tissue during increased production of bone matrix (2–12 weeks), probably due to a difference between the properties of the COOH-terminal and NH_2-terminal fragments. Biochemical studies have shown that NH_2-terminal DMP1 exists as a proteoglycan [19], whereas COOH-terminal DMP1 is highly phosphorylated [4]. In addition to these differences in biochemical properties, our immunohistochemical studies showed that NH_2-terminal DMP1 detected by antibodies specific for DMP1-1 and -2 was predominantly localized in osteocytes and the surrounding bone matrix, whereas COOH-terminal DMP1 detected by antibodies specific for DMP1-3 and -4 was predominantly localized in the pericanalicular matrix in mineralized bone. Maciejewska et al. [20] also reported differences in dental-tissue distribution of the NH_2- and COOH-terminal fragments: in their study, NH_2-terminal DMP1 was restricted to the non-mineralized regions of the tooth predentin, whereas COOH-terminal DMP1 was restricted to the mineralized tooth dentin. Thus, COOH-terminal DMP1 seems to be distributed in mineralized tissue. These differences in biochemical properties and tissue distribution may be related to the higher level of circulating COOH-terminal DMP1 relative to NH_2-terminal DMP1 during rapid growth, but our study has some limitation to understand it. Functional analyses using genetically engineered mice have shown that proteolytic processing of DMP1 is essential to bone formation and mineralization [21], and that the COOH-terminal DMP1 contains the functional domain that controls osteocyte maturation and bone mineralization [22]. Thus, circulating COOH-terminal DMP1, which can be measured by DMP1 ELISA 4–3, may represent a novel marker for osteocyte maturation and bone mineralization.

To explore the relevance of circulating DMP1 as a marker of bone metabolism, we compared levels of DMP1 and other biochemical markers of bone metabolism. We observed that DMP1 levels had the highest positive correlation with levels of Dkk-1, the second highest positive correlation with levels of osteocalcin, and lower positive correlations with levels of Trap5b and SOST. Because DMP1 levels had a high correlation with levels of osteocalcin (a well-known bone-formation marker) [23] and a lower correlation with levels of Trap5b (a well-known bone resorption marker) [24], DMP1 may be a marker of bone formation rather than bone resorption. Some investigators have suggested that osteocalcin is released during bone resorption because a large fraction of synthesized osteocalcin is incorporated into bone; therefore, osteocalcin is also considered to be a marker of bone turnover that indicates the balance between bone formation and resorption [25]. In comparison with osteocalcin produced by mature osteoblasts on the bone surface [26], DMP1 produced by osteocytes within the bone is even more fully incorporated into the inner bone. Therefore, DMP1 should be also released more specifically during bone resorption. We think that this is why DMP1 levels correlate not only the levels of osteocalcin but also the levels of Trap5b. Second, considering that Dkk-1 and SOST act as osteocyte-derived negative regulators of bone formation via inhibition of the Wnt signaling pathway [27–30], the high correlation between DMP1 and Dkk-1 levels and lower correlation between DMP1 and SOST levels are seemingly contradictory. However, the expression patterns of these proteins are not identical: Dkk-1 is expressed in osteoblasts and osteocytes [27], whereas SOST is expressed exclusively in osteocytes [29]. Thus, it is thought that Dkk-1 distributed in superficial bone is easily released into circulating blood, but that SOST distributed only in the inner portion of bone is not easily released into circulating blood. These differences in expression patterns of Dkk-1 and SOST may cause larger differences in the correlation rates between the levels of each protein pair. Third, the highest correlation between circulating Dkk-1 and DMP1 levels and the second highest correlation between circulating osteocalcin and DMP1 levels were observed in this study. These high correlations between the levels of each protein pair may be due to the similar expression patterns of these proteins. That is, osteocalcin is expressed in highly differentiated osteoblasts [26], Dkk-1 in osteoblasts and osteocytes [27], and DMP1 in immature osteocytes [1]. These proteins are expressed at transitional stage of osteoblast-to-osteocyte and distributed in superficial bone and are easily released from it, and hence the circulating levels of these proteins can show similar dynamic state. In addition, based on these situations, circulating DMP1 may be a marker of immature osteocytes rather than mature osteocytes. Further studies are needed to evaluate the significance of circulating DMP1.

Acknowledgments

This work was partially supported by JSPS KAKENHI (Grant-in-aid for Scientific Research), Grant Number 21390491.

Conflicts of interest

This work was supported by Research Foundation of Asahi Kasei Pharma Corporation. Y. Isogai and T. Kuroda are employees of Asahi Kasei Pharma Corporation. Y. Hagiwara and N. Maruyama are employees of Immuno-Biological Laboratories Co., Ltd.

References

[1] Toyosawa S, Shintani S, Fujiwara T, Ooshima T, Sato A, Ijuhin N, et al. Dentin matrix protein 1 is predominantly expressed in chicken and rat osteocytes but not in osteoblasts. J Bone Miner Res 2001;16:2017–26.

[2] Fisher LW, Torchia DA, Fohr B, Young MF, Fedarko NS. Flexible structures of SIBLING proteins, bone sialoprotein, and osteopontin. Biochem Biophys Res Commun 2001;280:460–5.

[3] George A, Sabsay B, Simonian PA, Veis A. Characterization of a novel dentin matrix acidic phosphoprotein. Implications for induction of biomineralization. J Biol Chem 1993;268:12624–30.

[4] Qin C, Brunn JC, Cook RG, Orkiszewski RS, Malone JP, Veis A, et al. Evidence for the proteolytic processing of dentin matrix protein 1 Identification and characterization of processed fragments and cleavage sites. J Biol Chem 2003;278:34700–8.

[5] Huang B, Maciejewska I, Sun Y, Peng T, Qin D, Lu Y, et al. Identification of full-length dentin matrix protein 1 in dentin and bone. Calcif Tissue Int 2008;82:401–10.

[6] Feng JQ, Ward LM, Liu S, Lu Y, Xie Y, Yuan B, et al. Loss of DMP1 causes rickets and osteomalacia and identifies a role for osteocytes in mineral metabolism. Nat Genet 2006;38:1230–1.

[7] Lorenz-Depiereux B, Bastepe M, Benet-Pagès A, Amyere M, Wagenstaller J, Müller-Barth U, et al. DMP1 mutations in autosomal recessive hypophosphatemia implicate a bone matrix protein in the regulation of phosphate homeostasis. Nat Genet 2006;38:1248–50.

[8] Seibel MJ. Molecular markers of bone turnover: biochemical, technical and analytical aspects. Osteoporos Int 2000;11(Suppl. 6):S18–29.

[9] Bonewald LF. The amazing osteocyte. J Bone Miner Res 2011;26:229–38.

[10] Tatsumi S, Ishii K, Amizuka N, Li M, Kobayashi T, Kohno K, et al. Targeted ablation of osteocytes induces osteoporosis with defective mechanotransduction. Cell Metab 2007;5:464–75.

[11] Robling AG, Niziolek PJ, Baldridge LA, Condon KW, Allen MR, Alam I, et al. Mechanical stimulation of bone in vivo reduces osteocyte expression of Sost/sclerostin. J Biol Chem 2008;283:5866–75.

[12] Qiu S, Rao DS, Palnitkar S, Parfitt AM. Reduced iliac cancellous osteocyte density in patients with osteoporotic vertebral fracture. J Bone Miner Res 2003;18:1657–63.

[13] Vashishth D, Verborgt O, Divine G, Schaffler MB, Fyhrie DP. Decline in osteocyte lacunar density in human cortical bone is associated with accumulation of microcracks with age. Bone 2000;26:375–80.

[14] Schneider P, Meier M, Wepf R, Müller R. Towards quantitative 3D imaging of the osteocyte lacuno-canalicular network. Bone 2010;47:848–58.

[15] Mark MP, Butler WT, Prince CW, Finkelman RD, Ruch JV. Developmental expression of 44-kDa bone phosphoprotein (osteopontin) and bone gamma-carboxyglutamic acid (Gla)-containing protein (osteocalcin) in calcifying tissues of rat. Differentiation 1988;37:123–36.

[16] Ikeda T, Nomura S, Yamaguchi A, Suda T, Yoshiki S. In situ hybridization of bone matrix proteins in undecalcified adult rat bone sections. J Histochem Cytochem 1992;40:1079–88.

[17] Chen J, Shapiro HS, Sodek J. Development expression of bone sialoprotein mRNA in rat mineralized connective tissues. J Bone Miner Res 1992;7:987–97.

[18] Olsen JV, Blagoev B, Gnad F, Macek B, Kumar C, Mortensen P, et al. Global, in vivo, and site-specific phosphorylation dynamics in signaling networks. Cell 2006;127:635–48.

[19] Qin C, Huang B, Wygant JN, McIntyre BW, McDonald CH, Cook RG, et al. A chondroitin sulfate chain attached to the bone dentin matrix protein 1 NH_2-terminal fragment. J Biol Chem 2006;281:8034–40.

[20] Maciejewska I, Cowan C, Svoboda K, Butler WT, D'Souza R, Qin C. The NH_2-terminal and COOH-terminal fragments of dentin matrix protein 1 (DMP1) localize differently in the compartments of dentin and growth plate of bone. J Histochem Cytochem 2009;57:155–66.

[21] Sun Y, Prasad M, Gao T, Wang X, Zhu Q, D'Souza R, et al. Failure to process dentin matrix protein 1 (DMP1) into fragments leads to its loss of function in osteogenesis. J Biol Chem 2010;285:31713–22.

[22] Lu Y, Yuan B, Qin C, Cao Z, Xie Y, Dallas SL, et al. The biological function of DMP-1 in osteocyte maturation is mediated by its 57-kDa COOH-terminal fragment. J Bone Miner Res 2011;26:331–40.

[23] Brown JP, Delmas PD, Malaval L, Edouard C, Chapuy MC, Meunier PJ. Serum bone Gla-protein: a specific marker for bone formation in postmenopausal osteoporosis. Lancet 1984;1:1091–3.

[24] Halleen JM, Hentunen TA, Karp M, Käkönen SM, Pettersson K, Väänänen HK. Characterization of serum tartrate-resistant acid phosphatase and development of a direct two-site immunoassay. J Bone Miner Res 1998;13:683–7.

[25] Ivaska KK, Hentunen TA, Vääräniemi J, Ylipahkala H, Pettersson K, Väänänen HK. Release of intact and fragmented osteocalcin molecules from bone matrix during bone resorption in vitro. J Biol Chem 2004;279:18361–9.

[26] Heersche JN, Reimers SM, Wrana JL, Waye MM, Gupta AK. Changes in expression of alpha 1 type 1 collagen and osteocalcin mRNA in osteoblasts and odontoblasts at different stages of maturity as shown by in situ hybridization. Proc Finn Dent Soc 1992;88(Suppl. 1):173–82.

[27] Li J, Sarosi I, Cattley RC, Pretorius J, Asuncion F, Grisanti M, et al. Dkk1-mediated inhibition of Wnt signaling in bone results in osteopenia. Bone 2006;39:754–66.

[28] MacDonald BT, Joiner DM, Oyserman SM, Sharma P, Goldstein SA, He X, et al. Bone mass is inversely proportional to Dkk1 levels in mice. Bone 2007;41:331–9.

[29] van Bezooijen RL, Roelen BA, Visser A, van der Wee-Pals L, de Wilt E, Karperien M, et al. Sclerostin is an osteocyte-expressed negative regulator of bone formation, but not a classical BMP antagonist. J Exp Med 2004;199:805–14.

[30] Poole KE, van Bezooijen RL, Loveridge N, Hamersma H, Papapoulos SE, Löwik CW, et al. Sclerostin is a delayed secreted product of osteocytes that inhibits bone formation. FASEB J 2005;19:1842–4.

Cell Biology:

Sympathetic Activation Induces Skeletal *Fgf23* Expression in a Circadian Rhythm-dependent Manner

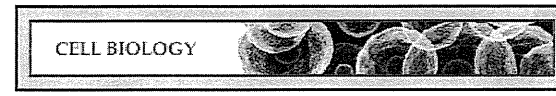

Masanobu Kawai, Saori Kinoshita, Shigeki Shimba, Keiichi Ozono and Toshimi Michigami

J. Biol. Chem. 2014, 289:1457-1466.
doi: 10.1074/jbc.M113.500850 originally published online December 3, 2013

THE JOURNAL OF BIOLOGICAL CHEMISTRY VOL. 289, NO. 3, pp. 1457–1466, January 17, 2014

Sympathetic Activation Induces Skeletal *Fgf23* Expression in a Circadian Rhythm-dependent Manner*[S]

Received for publication, August 1, 2013, and in revised form, November 18, 2013 Published, JBC Papers in Press, December 3, 2013, DOI 10.1074/jbc.M113.500850

Masanobu Kawai[‡1], **Saori Kinoshita**[‡], **Shigeki Shimba**[§], **Keiichi Ozono**[¶], **and Toshimi Michigami**[‡]

From the [‡]*Department of Bone and Mineral Research, Osaka Medical Center and Research Institute for Maternal and Child Health, 840 Murodo-cho, Izumi, Osaka 594-1101, Japan, the* [§]*Department of Health Science, School of Pharmacy, Nihon University, 7-7-1 Narashinodai, Funabashi, Chiba 274-8555, Japan, and the* [¶]*Department of Pediatrics, Osaka University Graduate School of Medicine, 2-2 Yamadaoka, Suita, Osaka 565-0871, Japan*

Background: The mechanism whereby the circadian clock regulates phosphate metabolism remains elusive.
Results: *Fgf23* expression is regulated by the time of food intake which involves the alteration in circadian profile of sympathetic activity.
Conclusion: The circadian network plays important roles in phosphate metabolism.
Significance: The sympathetic regulation of *Fgf23* expression may shed light on new regulatory networks that could be important for phosphate homeostasis.

The circadian clock network is well known to link food intake and metabolic outputs. Phosphorus is a pivotal nutritional factor involved in energy and skeletal metabolisms and possesses a circadian profile in the circulation; however, the precise mechanisms whereby phosphate metabolism is regulated by the circadian clock network remain largely unknown. Because sympathetic tone, which displays a circadian profile, is activated by food intake, we tested the hypothesis that phosphate metabolism was regulated by the circadian clock network through the modification of food intake-associated sympathetic activation. Skeletal *Fgf23* expression showed higher expression during the dark phase (DP) associated with elevated circulating FGF23 levels and enhanced phosphate excretion in the urine. The peaks in skeletal *Fgf23* expression and urine epinephrine levels, a marker for sympathetic tone, shifted from DP to the light phase (LP) when mice were fed during LP. Interestingly, β-adrenergic agonist, isoproterenol (ISO), induced skeletal *Fgf23* expression when administered at ZT12, but this was not observed in *Bmal1*-deficient mice. *In vitro* reporter assays revealed that ISO trans-activated *Fgf23* promoter through a cAMP responsive element in osteoblastic UMR-106 cells. The mechanism of circadian regulation of *Fgf23* induction by ISO *in vivo* was partly explained by the suppressive effect of Cryptochrome1 (Cry1) on ISO signaling. These results indicate that the regulation of skeletal *Fgf23* expression by sympathetic activity is dependent on the circadian clock system and may shed light on new regulatory networks of FGF23 that could be important for understanding the physiology of phosphate metabolism.

Phosphorus is an indispensable nutritional element involved in numerous biological processes such as cell signaling, energy homeostasis, and bone metabolism (1–4). The regulation of phosphate metabolism is an integrated process involving multiple organs and accumulating evidence has demonstrated the pivotal roles of fibroblast growth factor 23 (FGF23)[2] in phosphate metabolism (4–9). FGF23 is produced mainly by osteoblastic cells, including osteocytes, and functions as an endocrine factor to regulate genes involved in phosphate and vitamin D metabolism (4). The nodal point of the regulation of phosphate metabolism by FGF23 seems to primarily reside in the suppression of NaP_i-IIa/c expression and 1,25-dihydroxyvitamin D production in the kidney (4). Clinical evidence from genetic disorders in which mutations in the *FGF23* gene or mutations causing aberrant FGF23 signaling are associated with dysregulated phosphate metabolism has placed bone-derived FGF23 in the center of regulatory networks of phosphate metabolism (10–12). Hence, it is critical to understand the mode of the regulation of FGF23 expression in the skeleton to fully understand the physiological and pathological functions of FGF23 in phosphate metabolism. Although previous studies have revealed that 1,25-dihydroxyvitamin D can stimulate *Fgf23* expression in bone in part by directly activating the *Fgf23* gene promoter (13–15), the precise mechanisms by which skeletal *Fgf23* expression is regulated remain largely elusive. Because serum phosphate levels have been shown to exhibit circadian profile in humans, it is likely that phosphate metabolism is under the regulation of the circadian clock system (16–18); however, the precise mechanism by which the circadian clock network regulates phosphate homeostasis is still largely unknown.

The circadian clock network is an evolutionarily conserved process by which organisms adapt to environmental cues such as the availability of nutrients (19–21). For example, when food access is restricted in mice in the daytime (light phase) only, the expression profiles of circadian clock genes and circadian-reg-

* This work was supported by a grant from Sukoyaka Grant for Maternal and Child Health (to M. K.).
[S] This article contains supplemental Figs. S1 and S2.
[1] To whom correspondence should be addressed. Tel.: 81-725-56-1220; Fax: 81-725-57-3021; E-mail: kawaim@mch.pref.osaka.jp.

[2] The abbreviations used are: FGF23, fibroblast growth factor 23; AL, *ad libitum*; CRE, cAMP responsive element; CREB, CRE-binding protein; DP, dark phase; IBMX, 3-isobutyl-1-methylxanthine; ISO, isoproterenol; LP, light phase; PRO, propranolol; PTH, parathyroid hormone; RF, restricted feeding; ZT, zeitgeber time.

TABLE 1
Primer sequences for real-time RT-PCR

Gene	Forward Primer	Reverse Primer
Rev-erbα	5′-cccaacgacaacaacctttg-3′	5′-ccctggcgtagaccattcag-3′
Dbp	5′-caccgtggaggtgctaatga-3′	5′-gcttgacagggcgagatca-3′
Bmal1	5′-aggcccacagtcagattgaaa-3′	5′-ccaaagaagccaattcatcaatg-3′

ulated genes related to metabolic outputs have been shown to exhibit a phase shift so that the organisms can utilize ingested nutrients in a timely manner (19, 22–24). The central pacemaker of the circadian clock system is located at the suprachiasmatic nucleus in the hypothalamus and is integrated by multiple steps including transcriptional, translational, and post-translational mechanisms (20). Briefly, Clock (circadian locomotor output cycles protein kaput) heterodimerizes with Bmal1 (brain and muscle ARNT-like 1; also known as ARNTL) and induces the expression of *PER* (period circadian protein) and *CRY* (cryptochrome), which in turn suppresses Clock/Bmal1 transcriptional activity, thereby forming a 24-h feedback loop (20).

The mechanisms by which nutrient availability affects the circadian clock network still need to be determined; however both central and peripheral networks have been implicated as functional in this regulation (20). Centrally, the food-entrainable oscillator, which is anatomically different from the suprachiasmatic nucleus, has been considered to determine food-anticipatory behavior (20). Changes in the circadian profile of sympathetic activity may be one of the central mechanisms connecting food intake and metabolic outputs because food intake has been shown to be associated with enhanced sympathetic activity (25–28). In addition to central regulation, peripheral tissues also possess an oscillator that is synchronized with the central circadian system through retinal, hormonal, nutritional, and neuronal signals (29, 30). Recent advances in our understanding regarding the role of the peripheral oscillator have emphasized its importance in metabolic regulation (21). Furthermore, it has been well established that the circadian clock system in peripheral tissues is entrained by nutritional cues (21, 23). Taken together, these findings led us to hypothesize that phosphate metabolism was regulated by the circadian clock network through the modification of food intake-associated sympathetic activation, which may involve the action of the peripheral clock system.

In the current study, we tested our hypothesis that the circadian profile of circulating phosphate and FGF23 levels is determined by the time of nutrient availability by analyzing the circadian profile of skeletal *Fgf23* expression in mice where the timing of food intake was restricted during the light phase and found that light phase-restricted feeding altered the circadian expression profile of skeletal *Fgf23*, which was in part caused by changes in the circadian profile of sympathetic activity. In addition, we demonstrated that stimulation with a β-adrenergic receptor agonist induced *Fgf23* expression, which was suppressed by the overexpression of Cry1. These results underline the important roles of the circadian clock system in the regulation of phosphate metabolism.

EXPERIMENTAL PROCEDURES

Mice—C57BL/6J mice were purchased from CLEA Japan, Inc., and *Bmal1* knock-out mice on a C57BL/6J background were generated as reported previously (31). Mice were maintained on a 12-h:12-h light dark cycle (lights on at zeitgeber time (ZT) 0) in a pathogen-free animal facility with free access to water and standard chow (CE-2; CLEA Japan, Inc.), unless otherwise mentioned. The light phase restricted feeding regimen was carried out by allowing mice access to food for 6 h between ZT2 and ZT8. A control diet containing 0.6% phosphate and 1.0% calcium and a high phosphate diet containing 1.65% phosphate and 1.0% calcium were purchased from CLEA Japan, Inc. All animal studies were reviewed and approved by the Institutional Animal Care and Use Committee of Osaka Medical Center and Research Institute for Maternal and Child Health.

Reagents and Cell Lines—Isoproterenol hydrochloride, propranolol hydrochloride, and 3-isobutyl-1-methylxanthine (IBMX) were purchased from Wako Pure Chemical Industries Ltd. (Osaka, Japan). Human parathyroid hormone (PTH)(1–34) was obtained from the Peptide Institute, Inc. (Osaka, Japan). UMR-106 cells were obtained from ATCC (Manassas, VA) and maintained in DMEM supplemented with 10% fetal bovine serum and 1% insulin-transferrin-selenium-G supplement (Invitrogen). Cells were cultured at 37 °C in a 5% CO_2 atmosphere.

Real-time RT-PCR—Total RNA was prepared using TRIzol (Invitrogen) and treated with DNase I (Qiagen). cDNA was generated using a random hexamer and reverse transcriptase (Superscript II; Invitrogen) according to the manufacturer's instructions. The quantification of mRNA expression was carried out using a 7300 Real-time PCR system or a StepOnePlus™ Real-time PCR system (Applied Biosystems). TaqMan Gene Expression Assays for *Fgf23*, *Cryptochrome1*, *Rankl*, *Sost*, *Slc34a1*, *Slc34a3*, *Cyp27b1*, *Cyp24a1*, and *Gapdh* were purchased from Applied Biosystems. Primer sequences for *Rev-erbα*, *Dbp*, and *Bmal1* are described in Table 1. *Gapdh* was used as an internal standard control gene for all quantifications.

Western Blot Analysis—To prepare whole cell lysates, cells were solubilized in radioimmunoprecipitation assay buffer (1% Triton X-100, 1% sodium deoxycholate, 0.1% SDS, 150 mM NaCl, 10 mM Tris-Cl (pH 7.4), 5 mM EDTA, 1 mM orthovanadate, and protease inhibitor mixture (Complete™; Roche Diagnostics). Equal amounts of protein were separated by SDS-PAGE and transferred electrophoretically to PVDF membranes. Membranes were blocked in BlockAce reagent (Dainippon Pharmaceuticals, Osaka, Japan) or Blocking-one P reagent (Nacalai Tesque, Kyoto, Japan), immunoblotted with anti-CREB (1:1000, 9192; Cell Signaling, Beverly, MA), anti-pCREB (1:1000, 9191; Cell Signaling), anti-V5 (1:5000, 46-0705; Invitrogen), or anti-β-actin (1:2000, sc-47778; Santa Cruz Bio-